NBSIR 75-657 (R)

Report No. 7
A Metallurgical Investigation of a Full-Scale Insulated Rail Tank Car Filled With LPG Subjected to a Fire Environment

J. G. Early and C. G. Interrante

Mechanical Proper
Metallurgy Divisio
Institute for Mater
National Bureau of
Washington, D. C.

January 1975

Final Report

Prepared for

Federal Railroad Administration
Department of Transportation
Washington, D. C. 20591

NBSIR 75–657

Report No. 7
A METALLURGICAL INVESTIGATION OF A FULL-SCALE INSULATED RAIL TANK CAR FILLED WITH LPG SUBJECTED TO A FIRE ENVIRONMENT

J. G. Early and C. G. Interrante

Mechanical Properties Section
Metallurgy Division
Institute for Materials Research
National Bureau of Standards
Washington, D. C. 20234

January 1975

Final Report

Prepared for
Federal Railroad Administration
Department of Transportation
Washington, D. C. 20594

U. S. DEPARTMENT OF COMMERCE, Frederick B. Dent, Secretary

NATIONAL BUREAU OF STANDARDS, Richard W. Roberts, Director

TABLE OF CONTENTS

		Page
ABSTRACT		v
1.	INTRODUCTION	1
2.	PURPOSE	2
3.	EXPERIMENTAL PROCEDURES	3
	3.1 Macroscopic Observations and Thickness Measurements	3
	3.2 Chemical Analysis	3
	3.3 Metallographic Observations and Hardness Testing	4
4.	RESULTS AND DISCUSSION	4
	4.1 Chemical Composition	4
	4.2 Macroscopic Observations and Thickness Measurements	5
	4.3 Metallographic Analysis	7
	4.3.1 Shell Course 3	7
	4.3.2 Shell Course 1	9
	4.4 Hardness Measurements	10
	4.4.1 Shell Course 3	10
	4.4.2 Shell Course 1	10
	4.4.3 Stress-relieving Experiments	11
	4.5 General Discussion	12
5.	SUMMARY	16
6.	CONCLUSIONS	18
7.	ACKNOWLEDGEMENT	19

Table of Contents (Continued)

Page

REFERENCES 20

TABLES

I. Chemical Composition of Plate Samples from Insulated Tank Car RAX 202 . . . . . .

II. Macroscopic Observations of Plate Samples TC2-(1) and TC2-(3) from Shell Course 3 . . .

III. Hardness Data Summary . . . . . .

FIGURES

1. Insulated Tank Car RAX 202 positioned in the pit prior to initiation of the fire test . . . . .

2. Photographs of fragments of Tank Car RAX 202 after failure . . . . . .

3. Plate sample TC2-(1), shell course 3, taken from fragment C . . . . . .

4. Plate sample TC2-(3), shell course 3, taken from fragment C . . . . . .

5. Plate sample TC2-(7), shell course 4, taken from fragment B . . . . . .

6. Plate sample TC2-(10), taken from shell courses 1 and 2 of fragment A at the top of the tank car . . . . . .

7. Plate sample TC2(11) taken from shell courses 1 and 2 of fragment A at the bottom of the tank car . . . . . .

8. Schematic diagram showing the location of NBS samples in Tank Car RAX 202 . . . . . .

9. Schematic showing the three mutually perpendicular planes associated with the rolling direction in a steel plate . . . . . .

10. Close-up of a portion of the inside surface of plate sample TC2-(1) . . . . . .

FIGURES (continued)

11. Macrograph of fracture face of TC2-(1) between locations 5 and 6 . . . . . .

12. Macrograph of fracture face of TC2-(1) between locations 6 and 7 . . . . . .

13. Macrograph of inside plate surface of TC2-(1) at the fracture surface . . . . . .

14. Profile view of fracture surface on plate sample TC2-(7) . . . . . .

15. Profile views of fracture surface on plate sample TC2-(1), shell course 3 . . . . . .

16. Representative microstructure of plate sample TC2-(1) away from fracture face . . . . . .

17. Representative microstructure of plate sample TC2-(3) . . . . . .

18. Photomicrographs of plate sample TC2-(1) adjacent to hardness specimens . . . . . .

19. Photomicrographs of plate sample TC2-(3) adjacent to hardness specimens . . . . . .

20. Photomicrographs of the plate surfaces of plate sample TC2-(1) near the fracture surface . . .

21. Photomicrograph of an intergranular crack near the fracture initiation site on plate sample TC2-(1) . . . . . .

22. Photomicrographs of fracture surface of plate sample TC2-(1) . . . . . .

23. Photomicrographs of the fracture surface and region immediately behind . . . . . .

24. SEM fractographs of the fracture surface of plate sample TC2-(1) near outside plate surface . . . . . .

25. SEM fractographs of the fracture surface of plate sample TC2-(1) near midthickness region . . . . . .

FIGURES (continued)

26. SEM fractographs of the fracture surface of plate sample TC2-(1) near inside plate surface . . . .

27. Representative microstructures of plate sample TC2-(10B) . . . . . .

28. Representative microstructures of plate sample TC2-(11B) . . . . . .

29. Photomicrographs of plate sample TC2-(10B) adjacent to hardness specimens . . . . . .

30. Photomicrographs of plate sample TC2-(11B) adjacent to hardness specimens . . . . . .

31. Schematic of representative hardness profiles from plate samples TC2-(3) and TC2-(11B) . . . .

ABSTRACT

An analysis of the failure of an insulated rail tank car, RAX 202, which had been tested to failure in a fire environment at White Sands Missile Range, New Mexico, was requested by the Federal Railroad Administration, Department of Transportation.

The tank car, filled with approximately 33,000 gallons of liquified petroleum gas (LPG), failed after approximately 94 minutes of exposure to a JP-4 jet fuel fire. The car fractured into four fragments which were examined in the field. Five plate samples from the four fragments were selected for laboratory study at the National Bureau of Standards.

The results of laboratory check chemical analyses of five specimens representing three shell courses indicated that all of the samples tested met the chemical requirements of AAR TC128-B steel. The chemical variability between individual plate samples was low, and the levels of phosphorous and sulphur were notably low in comparison with the levels found in six heats of TC128 steels previously analyzed at NBS.

The results of metallurgical investigations suggest that a region approximately 30 inches in length near the top of the tank car in shell course 3 was the site of the initial rupture of the tank car. This rupture was attributed to the tensile hoop stress due to internal gas pressure, as the crack was aligned with the longitudinal axis of the tank car. The results of stress-relieving experiments conducted on samples taken from the top and bottom of the car indicated that the top of the tank car experienced temperatures of 1200°F to 1250°F for times of between 10 to 15 minutes.

The fracture features of the initial rupture were indicative of failure by a stress-rupture mechanism. It was concluded that this 30-inch stress-rupture crack led to tensile overload, instability and to the onset of rapid crack propagation in a shear mode, with the initial shear fracture propagating as an extension of the original stress-rupture crack. Within a short distance, this shear fracture turned 90° and propagated in the plate rolling direction, a result explained by the anisotropy of the fracture resistance of this steel at the elevated temperatures of the test. This reorientation occurred despite the fact that the hoop stress which promotes fracture in the longitudinal axis of the tank car is twice as large as the stress that promotes fracture along the rolling direction of the plate.

1. INTRODUCTION

A metallurgical evaluation of a full-scale railroad tank car tested to failure was requested by the Federal Railroad Administration, Department of Transportation. A fire test (Fire Test 2) was conducted on tank car RAX 202 on December 6, 1973, at White Sands Missile Range, New Mexico, under the direction of personnel from the United States Army Ballistic Research Laboratory. The tank car tested was similar to a standard 33,000 gallon tank car with the exception of three modifications. One modification was the addition of a second manway to provide access to the interior of the tank car in order to facilitate the installation of temperature and pressure sensors at various locations inside the tank car. Secondly, two ports were added to one side of the tank car through which the instrumentation cables passed, and finally, a white, protective, thermal coating was sprayed over the entire tank car. The steel plates used in the fabrication of tank car RAX 202 were reported to be 5/8 inch-thick, fine-grained steel plate in the as-rolled condition and to have been produced to Specification AAR M128-69, Grade B, Flange Quality, by the Lukens Steel Company as part of Melt Number CO 485.(1)

The tank car, filled with approximately 33,000 gallons of liquified petroleum gas (LPG), was placed in a large pit. A low earth dike that was continuously maintained at a level of about 18 inches of JP-4 jet fuel surrounded the tank car. When ignited, this pool of jet fuel, located beneath the tank car, provided the thermal energy to heat the tank car. Figure 1 shows the tank car positioned in the pit surrounded by the fuel dike prior to the fire test.(2)

The time to failure of the tank car was measured beginning with the ignition of the JP-4. At about 60 minutes into the test, the temperature and pressure recording systems failed. This failure prevented the recording of any temperature or pressure data for the remainder of the test. Approximately 94 minutes after ignition of the JP-4, the tank car failed and fractured into four fragments. Two fragments, constituting almost all of shell course 3, were propelled out of the pit. The smaller of the two fragments remaining in the pit contained the A head plate and shell courses 1 and 2, and the larger fragment remaining in the pit contained the B head plate and shell courses 4, 5, 6, and 7, see Figure 2.

A total of five steel-plate samples from four shell courses were selected, removed by torch cutting, and sent to NBS for metallurgical investigation. The samples, designated TC2-(1), TC2-(3), TC2-(7), TC2-(10)* and TC2-(11)*, were photographed in the as-received condition and are shown in Figures 3 through 7.

Plate sample TC2-(1), including the additional manway and encompassing the top of shell course 3, was torch-cut along the line BG (Figure 3). The fracture surface follows the line BCDEFG. Sample TC2-(3) was torch-cut from the bottom of shell course 3 and contains a portion of the fracture surface along HIJ (Figure 4), which is the continuation of the fracture BC in TC2-(1).

Plate sample TC2-(7), containing a portion of the girth weld which originally joined shell plates 3 and 4, was torch-cut from shell course 4, located in the larger remaining fragment in the pit, at the bottom of the tank car. A small piece of shell course 3, seen at the lower left front of the sample (Figure 5), contains part of the fracture surface, MNO, which is also an extension of the fracture surface BC in TC2-(1).

The last two plate samples, TC2-(10) and TC2-(11), were torch-cut from the smaller remaining fragment of the tank car in the pit. Sample TC2-(10), taken from the top of the tank car, and TC2-(11), taken from the bottom of the tank car directly opposite from TC2-(10), were selected for removal because they were from a relatively undeformed region of the tank car. A schematic of a portion of the tank car, Figure 8, shows a representation of the plate samples in their approximate location.

2. PURPOSE

The principal purpose of this metallurgical investigation was to determine the cause and location of the initial rupture which led to the fracture of the tank car. Another purpose of the investigation was to make observations of the fracture characteristics and the elevated-temperature mechanical behavior of this type of steel.

---

* Each of plate samples TC2-(10 and TC2-(11) contained portions of shell courses 1 and 2. Tests and observations of these two plate samples are reported here based on the particular shell course involved; TC2-(10A) and TC2-(11A) are from shell course 2 and TC2-(10B) and TC2-(11B) are from shell course 1.

3. EXPERIMENTAL PROCEDURES

Check chemical analyses of the plate samples were conducted for a comparison with the requirements of Specification AAR TC128-B-69. In addition, hardness surveys and thickness measurements were performed, and macroscopic and microscopic observations were made. Specimens for these tests and observations were taken from plate samples TC2-(1), TC2-(3), TC2-(10B) and TC2-(11B) with the following exceptions: (i) Chemical analysis was not performed on TC2-(10B) since TC2-(10B) and TC2-(11B) are from the same shell plate. (ii) Thickness measurements were not made on TC2-(10B) or TC2-(11B) because these two samples were taken from a shell plate that was not noticeably affected by the failure of the tank car. A chemical analysis was performed and macroscopic observations were made on sample TC2-(7).

Mechanical property measurements, including ambient- and hot-tensile tests, and stress-rupture tests, are currently being conducted and will be reported on in a subsequent report.

3.1 Macroscopic Observations and Thickness Measurements

The fracture surfaces of samples TC2-(7) and TC2-(1) were macroscopically examined and fracture profile sections were taken, perpendicular to the fracture surfaces, at the locations designated in Figures 4 and 10. Thickness measurements were taken at various locations near the fracture surfaces and at various distances perpendicular to the fracture face in samples TC2-(3); these measurements were used to determine if plate thinning occurred in regions near the fracture.

3.2 Chemical Analysis

Check chemical analyses (by combustion-conductometric, x-ray fluorescence, and emission spectroscopy methods) were conducted by a commercial testing laboratory at a quarter-thickness position of chemistry samples taken from plate samples TC2-(1) and TC2-(3) (shell course 3), TC2-(7) (shell course 4), and TC2-(11B) (shell course 1). The location of the chemistry samples on each of these plates is shown in Figures 3, 4, 5 and 7. Two chemistry samples, designated 1B and 1C, were taken from sample TC2-(1) for analysis. Sample 1B was taken from an area near what is believed to be the original rupture, and sample 1C was taken from an area as close as possible to the corner of the plate,* in accordance

---

* The shell plates are fabricated by forming flat rectangular plates into a cylindrical shape with the narrower plate ends abuting each other, and are joined by welding the narrow sides together. The plate corners are thus separated by this longitudinal seam weld.

with Specification ASTM A20-67, "General Requirements for Delivery of Steel Plates for Pressure Vessels", which specifies that check analyses samples shall be taken from a corner of the as-rolled plate.

3.3 Metallographic Observations and Hardness Testing

Representative photomicrographs, oriented as shown in Figure 9, were obtained on the metallographic specimens taken from plate samples TC2-(1), TC2-(3) (shell course 3), TC2-(10B) and TC2-(11B) (shell course 1). Metallographic observations were made on selected polished and etched areas of logitudinal C planes, shown in Figures 4, 6, 7 and 10. The ferrite grain size was measured in accordance with Specification ASTM E112-63, "Estimating the Average Grain Size of Metals". Scanning electron microscope (SEM) photographs were taken of the fracture face at a location indicated in Figure 10.

Rockwell B hardness measurements were taken on specimens adjacent to the metallographic specimens from plate samples TC2-(1), TC2-(3), TC2-(10B) and TC2-(11B). Hardness measurements were taken on transverse B planes (see Figure 9) at numerous locations on a 0.1-inch square grid in rows parallel to the plate surfaces in order to determine the average hardness of the specimens.

Additional groups of hardness specimens were prepared from plate samples TC2-(3) and TC2-(11B).* Room-temperature hardness measurements were taken on these specimens before and after annealing at various temperatures. These qualitative tests were conducted in order to estimate the temperature of the steel at the time of failure by matching the hardness values of the laboratory stress-relieved specimens taken from the bottom of the tank car with those of specimens in the as-received condition taken from locations near the top of the tank car.

4. RESULTS AND DISCUSSION

4.1 Chemical Composition

The chemical compositions, as determined by the commercial testing laboratory's check analyses of the five specimens from three shell courses, are given in Table I along with the producer's ladle analysis and the chemical requirements for AAR TC128-69 Grade B steel. The results of the laboratory check

---

* The individual specimens in each group were cut adjacent to each other and were located adjacent to the metallographic specimens.

analyses and the producer's ladle analysis are in good agreement, and they indicate that the composition of the five samples met the chemical requirements for AAR TC128-69 Grade B steel.

The compositional variability of samples taken from different locations within the same shell course, chemistry samples 1B, 1C and 3 (shell course 3), is quite low with the possible exception of the manganese and sulfur levels in sample 3, which are below the mean value obtained from the other two samples. The compositional variability between these samples and those from other shell courses, chemistry sample 7 (shell course 4) and chemistry sample 11B (shell course 1) is also low and is consistent with the fact that all of the plates for tank car RAX 202 were produced from the same heat of steel.

The aluminum check analyses showed that the steel was deoxidized by a combination of silicon and aluminum, indicating that the steel was produced in accordance with fine-grain practice. Vanadium was not detected by either the producer's ladle analysis or by the check analysis. This result confirms that the plates are Grade B steel, and it indicates that the steel does not meet the minimum vanadium requirement of 0.02 percent-by-weight for Grade A steel.

The levels of sulfur and phosphorus are particularly low, averaging respectively 0.013 and 0.006 percent-by-weight for the five check analyses. These values compare with average check analysis values of 0.026 and 0.018 percent-by-weight for six steel samples taken from failed tank cars and tested at NBS.(3) When compared with these six plate steels, the relatively low level of phosphorus would be expected to give lower impact transition temperatures, and the relatively low level of sulfur would be expected to increase the upper-shelf energy absorption values in impact tests of the steel. The upper-shelf energy absorption values are important to the elevated-temperature crack propagation behavior of the steel, and in particular it is believed that they may relate to the critical flaw size for initiation of ductile fracture.

4.2 Macroscopic Observations and Thickness Measurements

Macroscopic examination of plate samples TC2-(3), TC2-(7), and TC2-(11) revealed that the outside surfaces of these plates were either partially or completely covered with the charred remnant of the protective thermal coating. Plate samples TC2-(3) and TC2-(11) contained an inner layer of uncharred thermal coating next to the outside plate surface and an outer charred layer. These samples were taken from locations on the bottom of the tank car where the fire exposure apparently was insufficient to burn off or completely char the thermal coating.

Approximately one-half of the outer plate surface of sample TC2-(7), the half closest to the bottom of the tank car, was covered with the charred coating residue, while the other half of TC2-(7) was completely free of any coating residue. These findings are consistent with the observations for TC2-(3) and TC2-(11). Examination of samples TC2-(1) and TC2-(10) revealed that their outside surfaces were completely free of the thermal coating. These two plate samples were removed from the top of the tank car, where the fire exposure was apparently sufficient to burn off the thermal coating.

The fracture face of sample TC2-(1) was examined before specimens for other studies were cut from this sample. Macrographs of the fracture surface between locations 5 and 7 (Figure 10) are shown in Figures 11 and 12. The fracture appearance shown in Figure 10 is typical of that observed along the region from midway between locations 4 and 5 to midway between locations 7 and 8.

The inside and outside plate surfaces of TC2-(1) near the fracture surface were examined. Numerous secondary cracks adjacent to and running parallel with the fracture face were observed between locations 4 and 8 (Figure 10) on both the inside and outside surfaces. Within a length of six inches on either side of location 5, secondary cracks were found in an area extending about one inch back from the fracture face. In the other regions, the secondary cracks were confined to within one-half inch of the fracture face. Figure 13, taken near location 5, shows a portion of the fracture face and the adjoining inside plate surface with a large number of the secondary cracks being visible on the plate surface.

Two fracture modes were observed along the fracture face of plate sample TC2-(1). One mode was characterized by a fracture surface nearly perpendicular to plate surfaces, and the other fracture mode, a shear type, was characterized by a fracture surface inclined at an angle of about 45° to the plate surfaces. Samples TC2-(3) and TC2-(7) contained only the shear mode. Profile views illustrating the two fracture modes are shown in Figures 14 and 15.

The fracture mode from B and C and from F to G (Figure 3) in sample TC2-(1) is a shear type with the fracture plane at an angle of about 45° with the surfaces of the plate and with one edge of the fracture plane in a weld HAZ, as represented by Figure 14b. A shear mode was also observed from C to D and from E to F, in both of which the fracture surface lies entirely in base metal and makes an angle of about 45° with the plate surfaces, as represented by Figure 14a. Profile views of the fracture surface

between D and E, near locations 5 and 6, are shown in Figure 15. This fracture surface, although rough in appearance, is macroscopically nearly perpendicular to the plate surfaces with small protrusions, resembling shear-lips, being present at both the inside and outside plate surfaces.

Plate sample TC2-(3) contains another portion of the fracture face separating shell course 3 and shell course 4. The fracture mode from H to I (Figure 4) is a mixed type, represented by Figure 14c, with both perpendicular and shear regions, and with one edge of the fracture plane anchored in a HAZ. From I to J, the fracture mode is a shear type with one edge of the fracture plane in a HAZ.

Plate sample TC2-(7) contains a portion of the fracture surface which intersects the circumferential weld joining shell course 4 to shell course 3. The fracture mode from M to N (Figure 5) is a shear type with the fracture plane at an angle of 45° to the plate surfaces while from N to O the fracture mode is a mixed type. The fracture surfaces from M to N and from N to O are illustrated by Figures 14a and 14c, respectively.

Thickness measurements taken at various locations on the fracture surface of plate samples TC2-(1) and TC2-(3) indicate that substantial plate thinning occurred only between locations 3 1/2 and 9 on plate sample TC2-(1), Figure 10. Plate thinning, as measured by percent reduction in plate thickness, reached a maximum of almost 40% near location 5 and dropped off to 20% at locations 3 1/2 and 9. A tabulation of the fracture mode observations and plate thinning calculational results are given in Table II.

4.3 Metallographic Analysis

4.3.1 Shell course 3

Representative photomicrographs taken at low magnification on logitudinal C planes of plate samples TC2-(1) and TC2-(3) from shell plate 3 are shown in the etched condition in Figures 16 and 17, respectively. Sample TC2-(3) was taken from the bottom of the tank car, and sample TC2-(1) was taken from near the top of the tank car. The microstructure of TC2-(1) represents a region approximately two inches from the fracture surface. The photomicrographs reveal evidence of decarburization to a depth of about 0.005 inches on both surfaces. The presence of decarburization on the inside plate surface indicates that the observed decarburization on both surfaces probably occurred prior to the fire test, perhaps during the plate-rolling operation or the stress-relieving operation after the plates were welded together. These surface layers are primarily ferrite with very small amounts of pearlite. The tensile strength of these ferrite

surface layers is expected to be lower than that of the bulk of the plate, and these surface layers are therefore expected to have lower resistance to stress-rupture failure.

The microstructures of these two specimens are typical of a carbon-manganese steel in the hot-rolled condition. The microstructure consists of a mixture of proeutectoid ferrite and pearlite with moderate banding, of alternate layers of ferrite and pearlite, primarily in the midthickness region of the plate. The ferrite grain size number for both plate samples was determined to be 8 1/2, indicating that the proper fine-grain deoxidation practice was followed, and more importantly, indicating that either the finishing temperature of the plate rolling operation was low enough to preserve the fine austenite grain size which then transformed into a fine grain ferrite, or the cooling rate through the transformation temperature was sufficiently high to produce a high ferrite nucleation rate.

Photomicrographs taken of these two specimens at higher magnification are shown in Figures 18 and 19. The pearlite lamellae in plate sample TC2-(1), shown at a magnification of 500X in Figure 18a, are not clearly resolvable. At a magnification of 1250X, Figure 18b, regions within some pearlite colonies are shown to have retained their lamellar morphology while substantial areas have not, because spheroidization of the iron carbide phase has started. Figure 19a shows that in sample TC2-(3), regions of lamellar pearlite are clearly resolved at a magnification of 500X.* At a magnification of 1250X, Figure 19b, most pearlite colonies are seen to have regions of lamellar morphology.

A metallographic examination of the fracture surface and adjacent regions near location 6 (Figure 10) of sample TC2-(1) was conducted. The secondary cracks observed on the outside and inside surfaces near the fracture face generally lie at an angle of 45° to the surface as seen in Figure 20. Large numbers of fissures or voids are present, some of which are aligned ahead of advancing secondary cracks. The photomicrographs reveal the elongation of the ferrite grains as the plate thickness

---

* The ability to resolve at a given magnification the lamellar morphology of pearlite depends not only on the interlamellar spacing but also on the extent to which the microstructure has been modified by thermal treatment; e.g., iron carbide spheroidization. Since TC2-(1) and TC2-(3) are from the same steel plate where the austenitizing temperature and cooling rate through the transformation temperature are expected to be similar, the average interlamellar spacing in both TC2-(1) and TC2-(3) should be similar. The inability to resolve the pearlite at a magnification of 500X in TC2-(1) suggests that additional deterioration of the lamellae has occurred in plate sample TC2-(1) compared to plate sample TC2-(3).

decreased under the applied stress. The character of these secondary cracks can more easily be seen by looking at a small crack at high magnification. Figure 21, taken of a region on the inside plate surface, shows the crack to be intergranular and following interfaces between the ferrite and pearlite. The microstructure of the fracture profile, Figure 22, shows extensive elongation of the ferrite combined with the general degradation of the structure by the formation of large numbers of extensive voids in the vicinity of the fracture surface. Higher magnification micrographs of the region shown in Figure 22b shows that the fissures and voids form primarily at grain boundaries and particularly at the interface between proeutectoid ferrite and pearlite (see Figure 23).

SEM fractographs were taken of the fracture surface near location 6 of TC2-(1) (Figure 10), as this region was believed to have been part of the initial rupture. Evidence of fissures or cavities (Figures 24, 25 and 26) can be seen throughout the fracture interface from the outside plate surface to the inside plate surface. Higher magnification fractographs, Figures 24b, 25b, 26b and 26c, reveal a general dimpled appearance throughout the fracture interface. The dimpled character of the fracture interface indicates that ductile fracture occurred with extensive microvoid initiation and coalescence. It is often observed that overload fractures due to stress-rupture are initiated by microvoids at grain boundary junctions.(4) Additional active sites for microvoid nucleation are inclusions, microcracks, and interfaces between the matrix and particles such as carbides. The proeutectoid ferrite to pearlite interface could provide excellent sites for microvoid initiation. The observation that the small secondary cracks on the plate surfaces are intergranular in character is additional evidence that this fracture surface region was the origin of the initial rupture, and that failure of this region occurred by stress rupture through a combination of intergranular fracture and microvoid coalescence.

4.3.2 Shell course 1

Representative photomicrographs taken at low magnification on the logitudinal C planes of plate samples TC2-(10B) and TC2-(11B) from shell course 1 are shown in Figures 27 and 28. These microstructures indicate, as in the case of the shell course 3 specimens, that decarburization has occurred on both surfaces to a depth of about 0.005 inches. The inside and outside surface layers are therefore primarily ferrite compared to the bulk microstructure, and this is additional evidence that this decarburization preceded the fire test.

The microstructures are typical of AAR TC128-B steel in the as-rolled condition with a mixture of proeutectoid ferrite and pearlite with a lesser degree of banding than was observed in the shell course 3 specimens. The ferrite grain size numbers were 8 and 8 1/2 for TC2-(10B) and TC2-(11B) respectively, indicating that the grain-refining deoxidation practice was preserved by proper finishing temperature during the plate rolling operation.

Photomicrographs were taken of these two specimens at higher magnification to determine what differences, if any, existed between a specimen from the top region (hotter) of the tank car and a specimen from the bottom region (colder) of the tank car. The microstructures of TC2-(10B) and TC2-(11B) are similar, contrary to the observations made on the specimens from the fractured shell plate, shell course 3. Figures 29 and 30 reveal that, in both TC2-(10B) and TC2-(11B), the pearlite colonies retained substantial regions of lamellar morphology throughout the microstructure indicating that the exposure to elevated temperature during the fire test was insufficient to cause significant additional spheroidization of the iron carbide phase in the pearlite, even at the top of the tank car in this region of this shell course.

4.4 Hardness Measurements

Representative hardness measurements were taken on specimens from plate samples TC2-(1) and TC2-(3) taken from near the top and the bottom, respectively, of shell course 3 and on specimens from plate samples TC2-(10B) and TC2-(11B) taken from the top and bottom, respectively, of shell course 1. The results are summarized in column 3 of Table III.

4.4.1 Shell course 3

The average hardness for TC2-(3), taken from the bottom of the tank car, is R_B 89. This hardness corresponds to an approximate tensile strength of 87,000 psi.(5) The average hardness for TC2-(1), taken from near the top of the tank car, is R_B 86 1/2, corresponding to an approximate tensile strength of 82,000 psi.

4.4.2 Shell course 1

The average hardness for TC2-(11B), taken from the bottom of the tank car, is R_B 89, corresponding to an approximate tensile strength of 87,000 psi. The average hardness for TC2-(10B), taken from the top of the tank car, is R_B 88, corresponding to an approximate tensile strength of 86,000 psi.

These results show that the two plate samples, TC2-(3) and TC2-(11B), which were heated the least during the fire test, have the highest average hardness values. Plate sample TC2-(1), taken from the failed shell course in the region experiencing the highest temperature during the test, the top of the tank car, has the lowest average hardness value. Plate sample TC2-(10B) taken from the top of the tank car in shell course 1, which did not fail, has only a slightly lower average hardness value than TC2-(11B), taken from the bottom of the tank car. The difference in average hardness between TC2-(1) and TC2-(10B), samples from two different shell courses, can arise not only from metallurgical variables, such as the pearlite lamellae spacing prior to the fire test or the chemical composition, but also as a result of differing temperature-time environments experienced by different regions of the tank car during the fire test. Possibly the maximum temperature reached during the fire test or the time at temperature may have varied along the length of the tank car.

4.4.3 Stress-relieving Experiments

The hardness data used to determine the representative hardness values of each of four plate samples were found to vary depending on whether the measurements were near the two plate surfaces or in the midthickness region. This observation is not surprising since the metallographic study revealed moderate banding, principally in the midthickness region, in all of the plate samples. Thus, for a meaningful comparison, the hardness data must be compared from the same region of each test specimen. The grid network and the hardness row identification are illustrated in a schematic of two typical hardness specimens, Figure 31.

A simple set of experiments was conducted in an effort to duplicate the lower hardness values measured on specimens taken from TC2-(1) and TC2-(10B), from the top of the tank car, by stress-relieving specimens taken from TC2-(3) and TC2-(11B), from the bottom of the tank car, at various temperatures and times.* The results of these tests are summarized in columns 4, 5, and 6 of Table III.

---

* Although both time and temperature are independent variables which can affect the microstructure and thus the hardness of a specimen, the particular set of time-temperature parameters chosen were based on an estimate of the temperature and time-at-temperature of the top of the tank car. It should be remembered, however, that a microstructural change for a specific time-temperature combination will occur in a shorter time at a higher temperature.

The results for the specimens from the failed shell course, shell course 3, indicate that a 1221 F heat treatment for 15 minutes decreased the average hardness of TC2-(3) specimens by 2 R_B points, whereas the difference between TC2-(3) and TC2-(1) is 2 1/2 R_B points. The 1221 F treatment was thus insufficient to match the decrease in hardness, and either a longer time or slightly higher temperature would be required for a decrement of 2 1/2 R_B points.

The results for the specimens from an unfailed shell course, shell course 1, indicate that to reduce the hardness of TC2-(11B) specimens to the level of TC2-(10B), it would be necessary to heat into the temperature range of 1215 F to 1257 F for periods of 10 to 15 minutes: the difference in average hardness values between TC2-(11B) and TC2-(10B) is 1 R_B, whereas with a 1215 F heat treatment for 10 minutes the average hardness was lowered by 1/2 R_B, and with a 1257 F treatment of 15 minutes the average hardness was decreased by 1 1/2 R_B. The 1215 F heat treatment for a somewhat longer time would probably be sufficient to match the decrease in hardness found as a result of the fire test.

The larger difference in hardness values between TC2-(1) and TC2-(3) than between TC2-(10B) and TC2-(11B) is consistent with the microstructural observation that TC2-(1) contained greater iron carbide spheroidization than TC2-(3) while little difference was observed between TC2-(10B) and TC2-(11B). Thus, as expected, the plate tempered more severely had both a greater loss in hardness and a greater degree of spheroidization.

These stress-relief test results further show that at any temperature in excess of 1000°F, the specimens from shell course 3 were softer and thus weaker then those from shell course 1. Thus, of the two shell plates, shell course 3 would be expected to fail by stress-rupture before shell course 1 at a given temperature.

4.5 General Discussion

The purposes of this investigation were to determine the probable cause and location of the initial rupture which led to the initial fracture and eventually to complete failure of tank car RAX 202, and to make observations on the fracture characteristics and on elevated temperature behavior of AAR TC128-B steel.

To these ends plate samples from four shell courses were selected for laboratory investigation: a) the shell course that fractured and failed, shell course 3, b) part of an adjoining shell course, shell course 4, and c) two shell courses that did not fail, shell course 1 and shell course 2.

All of the steel plates in tank car RAX 202 were formed from a single heat of steel. The results of the check chemical analyses from the plate samples combined with the producer's ladle analysis of the melt indicated that all of the samples tested met the respective chemical requirements of AAR TC128-B steel. In addition, the variability on an elemental basis between individual shell plates and between the shell plates and the heat of steel was low. In chemical terms, the plate samples tested appear normal and barely distinguishable from each other.

Examination of the fracture edges of plate samples TC2-(1), TC2-(3) and TC2-(7) indicated that only two fracture modes were present, a shear mode with the fracture plane at an angle of 45° to the plate surfaces and a nearly perpendicular mode. The fracture mode in the region midway between locations 4 and 5 to midway between locations 7 and 8 on TC2-(1) (Figure 10), although exhibiting ductile behavior as evidenced by the substantial percent reductions in plate thickness (20% to 40%), has a rough irregular surface oriented approximately 90° to the plate surfaces.

Metallographic examination established the intergranular character of small secondary surface cracks running parallel to the fracture surface between locations 4 and 8 (Figure 9). In addition, micrographs taken of regions just behind the fracture face revealed substantial numbers of fissures or voids primarily originating at the interface between the proeutectoid ferrite and pearlite. SEM fractographs confirmed the ductile character of the fracture interface by the presence, throughout the fracture face of dimples formed by microvoid coalescence. The ferrite grain size was comparable to the size of the dimples, so that the SEM fractographs could not confirm the intergranular nature of the fracture face.

These combined results strongly suggest that the region midway between locations 4 and 5 to midway between locations 7 and 8 on TC2-(1) (Figure 10), approximately 30 inches long, was the site of the initial rupture of the tank car. The features of this fracture region are characteristic of failure by a stress-rupture mechanism. This type of failure occurs as a result of a high tensile stress being sustained for a sufficient time to reduce the net cross-sectional area of the plate to such an extent that the remaining ligaments of metal are insufficient to carry the applied load, with the result being failure by tensile overload. In this process, as intergranular void formation and coalescence progresses, the remaining ligaments of metal are subjected to an ever increasing

tensile stress. Concurrently with void formation and coalescence, cracks are formed and plate thinning occurs as a consequence of these plastic processes, resulting in a reduction in the plate cross-sectional area and this decreases the applied load necessary to cause tensile overloading.

Many of the small stress-rupture cracks eventually joined together to form a part-through crack at one or more locations. Subsequently, cracks completely penetrating the cross-section formed and grew until the length of the stress-rupture crack exceeded the critical value required for the onset of rapid crack propagation. For the steel of shell course 3, the 30 inch stress-rupture crack apparently exceeded this critical length for the stress level present at the time of the initial rupture.

The ultimate catastrophic failure and complete separation of shell course 3 from the tank car was probably the result of three cooperative events. First, the stress-rupture crack led to the initiation of rapid crack propagation. Secondly, as the gas pressure in the tank car was being relieved by the opening and further propagation of the cracks, the portions of the shell course adjacent to the cracks were rapidly forced apart by the force of the escaping gas, with the momentum of these large masses of metal providing additional energy to drive the crack propagation. Finally, as a result of the rapid opening of the tank car by the progressing fracture, a critical mixture of air and LPG at or near the crack opening occurred and was ignited by the fire, resulting in the explosion which completed the fracture and caused the fragments of shell course 3 to be propelled out of the pit.

The rapid crack propagation occurred by a shear mode. This mode, observed on plate samples TC2-(3), TC2-(7), and outside of the stress-rupture fracture on TC2-(1), was generally a ductile shear type with the fracture plane at 45° to the plate surfaces and reductions in plate thickness of between 10 and 20 percent. However, when the shear fracture followed a weld HAZ, it contained some regions nearly perpendicular to the plate surface and reductions in plate thickness of less than 10 percent.

The shear fracture paths were in general related to the circumferential or firth welds joining shell course 3 to shell courses 2 and 4. The initial shear fractures, propagating from each end of the stress-rupture crack, occurred with fracture planes transverse to the plate rolling direction. However, within a very short distance, near locations 3 1/2 and 8, the shear fracture planes began to curve and align themselves parallel to the plate rolling direction; i.e., the

longitudinal plate direction. During this reorientation process from the transverse to the longitudinal direction, one edge of the shear fracture plane reached the HAZ of each of these two girth welds, and then propagated near and parallel to these HAZ regions until the crack circumscribed the tank car. The reorientation of these propagating cracks from the transverse to the longitudinal direction of the plate is consistent with the findings of dynamic-tear (DT) tests at elevated temperatures on AAR TC128-B steel which indicated that the resistance to crack propagation in the direction transverse to the plate rolling direction is much greater than in the direction parallel to the plate rolling direction.(6) Over a broad range of elevated temperatures, the impact energy absorption of longitudinal specimens (transverse crack propagation) was as much as twice as large as that for transverse specimens (longitudinal crack propagation).

The shear cracks propagated in the circumferential direction despite the fact that the tensile stress due to the internal gas pressure in the tank car is twice as large in the circumferential direction (hoop stress) as in the axial direction. The large hoop stress should promote crack propagation along the length of the tank car. However, the anisotropy of fracture toughness of this steel can be large at elevated temperatures and this anisotropy apparently governed the crack propagation behavior, even for a crack that was initially propagating in a direction perpendicular to the "weaker" direction.

The results of the stress-relieving experiments show that the decrease in hardness found in specimens taken from two different shell plates at the top of the tank car TC2-(1) and TC2-(10B), can be explained if it is assumed that the top of the tank car experienced temperatures between 1200°F and 1250°F for times of between 10 to 15 minutes. The results of the fire test(7) on an uninsulated tank car, indicate that skin temperatures of the order of 1200°F can be achieved from the JP-4 fire and that flame temperature differences of over 300°F along the top of the tank car were measured. Since other combinations of temperature and time-at-temperature can lead to the observed decrease in hardness, the results of the stress-relieving study cannot be used to determine the actual shell plate temperature at the time of the initial rupture.

5. SUMMARY

1. An insulated tank car (RAX 202), which was fabricated from plates from a single heat of TC128-B steel, was tested to failure in a JP-4 fire environment. Five steel samples selected for this investigation were taken from the failed tank car and were designated TC2-(1), TC2-(3), TC2-(7), TC2-(10), and TC2-(11).

2. The plate samples selected for investigation were taken from four shell courses. Two samples were taken from shell course 3, the only shell course that failed in the fire test, TC2-(1), which contained what is believed to be the site of the original rupture near the top of the car, and TC2-(3), which was located at the bottom of the tank car in this failed shell course. Sample TC2-(7), contained portions of shell course 4 and the girth weld that joined shell courses 3 and 4. Portions of shell courses 1 and 2 were contained in each of two samples, TC2-(10) and TC2-(11), taken from relatively undeformed regions at the top and bottom of the tank car, respectively.

3. The chemical compositions of the samples taken from shell courses 1, 3, and 4 met the chemical requirements of AAR TC128-69, Grade B steel. The chemical variability on an elemental basis was low, both between individual plate samples and between the check chemical analyses of the plates and the ladle analysis of the heat.

4. Macroscopic examination of the outside plate surfaces of the samples indicated that exposure to the JP-4 fire was apparently insufficient to completely burn-off the protective thermal coating from samples located at the bottom of the tank car but the fire exposure was sufficient to completely burn-off the thermal coating from samples located at the top of the tank car.

5. Three of the five plate samples contained portions of the fracture surfaces. Examination of these fracture surfaces indicated that two distinct fracture modes are present. The fracture mode in one region near the top of the tank car in shell course 3, was rough and irregular with the fracture surface nearly perpendicular to the plate surfaces. This region is believed to be a 30-inch long stress-rupture crack and the origin of the failure of the tank car. Essentially all of the balance of the fracture occurred predominately by a shear mode with the fracture plane at an angle of about 45° to the plate surfaces.

5. Macroscopic observations revealed that, on both surfaces of the plate near the fracture face of the stress-rupture crack, numerous small cracks were present and they were aligned parallel with the stress-rupture crack.

7. Thickness measurements indicated that substantial plate thinning (20% to 40%) occurred only in and nearby the region of the stress-rupture crack. Reductions in plate thickness of between 10 and 20 percent were measured in the shear fracture regions, except that reductions in thickness of less than 10% were measured where the fracture surface followed a weld HAZ.

8. Results of metallographic examinations indicated that the stress-rupture crack was initiated by intergranular voids which formed primarily at interfaces between proeutectoid ferrite and pearlite. Scanning electron microscope fractographs indicated that this fracture surface was formed by void coalescence which led to ductile dimpled rupture throughout the cross section of the plate.

9. Metallographic examinations indicated that in the failed shell course (no. 3) a greater degree of iron-carbide spheriodization had occurred in the sample taken from the top of the car when compared with that for the sample taken from the bottom. In an unfailed shell course (no. 1), the exposure to elevated temperature was insufficient to cause significant differences in the level of iron-carbide spheroidization between samples taken from the top and bottom of the tank car.

0. The results of hardness measurements showed that the plate samples taken from the bottom of the tank car (in shell courses 1 and 3) had higher hardness values than those taken from the top of the tank car in these shell courses. The plate sample from the top of the tank car in the failed shell course (no. 3) had the lowest average hardness. Further, the plate sample from the top of the tank car in shell course 1, which did not fail, had only a slightly lower average hardness than the sample taken from the bottom of the tank car in this course. These hardness results are consistent with results of the metallographic observations of the relative levels of iron-carbide spheroidization.

11. The results of stress-relieving experiments on specimens from the failed shell course, shell course 3, indicated that with a heat treatment at 1221°F for 15 minutes, the average hardness of specimens from the tank car bottom

could be decreased by 2 R_B points, which is slightly less than the 2 1/2 R_B hardness difference measured between specimens taken from the top and bottom of this shell course. Similar experiments on specimens from an unfailed shell course, shell course 1, indicated that on specimens taken from the bottom of the car, heat treatments of 1215°F for 10 minutes and 1257°F for 15 minutes, respectively decreased the average hardness by 1/2 and 1 1/2 R_B points, whereas the average difference in hardness measured between specimens from the tank car top and bottom was 1 R_B point.

12. Extension of the initial rupture occurred by shear fracture which initially was aligned in the same direction as the stress-rupture crack, transverse to the plate rolling direction. Within a short distance from either end of the stress-rupture crack, the ends of this propagating shear crack turned 90° and propagated (still by shear fracture) in the plate rolling direction. During this reorientation process, from transverse to longitudinal, one edge of each of the two shear fracture planes reached the HAZ of a girth weld and propagation continued near to and parallel to these girth welds until the fracture circumscribed the tank car.

6. CONCLUSIONS

1. The insulated rail tank car failed by rupture of the third shell course after extended exposure to fire, with the initial rupture being a stress-rupture crack of about 30 inches in total length that was oriented parallel to the longitudinal axis of the tank car.

2. Growth of this stress-rupture crack occurred by a shear mode initially in the same direction as the stress-rupture crack, transverse to the plate rolling direction. After propagating a short distance, the shear fracture plane began to turn and the shear crack propagated in hoop direction of the tank car, parallel to the plate rolling direction.

3. This shear-fracture plane reorientation behavior is believed to be due to the anisotropy of the fracture resistance of this steel at elevated temperatures.

4. Hardness values of samples from the top and bottom of shell course 3 differed by a wider amount than did hardness values between specimens from the top and bottom of shell course 1 and this observation is consistant with the

microstructural observation that a larger degree of iron-carbide spheroidization occurred in the specimens from the top of shell course 3 than occurred in specimens from the top of shell course 1.

5. In both shell courses 1 and 3, the average hardness of specimens taken from the top of the tank car was less then that for specimens from the bottom of the car and this can be explained by differences in temperature and time-at-temperature experienced by these regions as a result of the fire exposure. The top of the tank car probably experienced temperatures between 1200°F and 1250°F for times of between 10 and 15 minutes. The bottom of the tank car is believed to have received insufficient high temperature exposure to cause a measureable decrease in the strength of the steel.

6. Shell course 3 would probably fail by a stress-rupture mechanism before shell course 1 at a given temperature of exposure due to the relative strengths of these two plates. The stress-relieving test results indicate that at temperatures above 1000°F shell course 3 specimens would be softer and thus weaker than the shell course 1 specimens.

7. ACKNOWLEDGEMENT

The author wishes to thank Dr. J. H. Smith for his comments and suggestions, and Mr. D. E. Harne for his able assistance in the metallographic and photographic portions of this report.

REFERENCES

1. Test Certificate, Lukens Steel Company, Mill Order Number 64931 1, Melt CO485, AAR-TC-128 GR. B, APPENDIX M FLG. 81000, February 29, 1972.

2. W. Townsend, C. Anderson, J. Zook, and G. Cowgill, "COMPARISON OF THERMALLY COATED AND UNINSULATED RAIL TANK CARS FILLED WITH LPG SUBJECTED TO A FIRE ENVIRONMENT", B.R.L. Interim Memorandum Report No. 319, USA Ballistic Research Laboratories, Aberdeen Proving Ground, Maryland, December 1974.

3. C. G. Interrante, J. G. Early, and G. E. Hicho, "ANALYSIS OF FINDINGS OF FOUR TANK CAR ACCIDENT REPORTS", (Report No. 5), To be published.

4. Metals Handbook Volume 9, The American Society for Metals, Metals Park, Ohio, 1974, p.75.

5. Army-Navy Approximate Hardness Tensile Strength Relationship of Carbon and Low Alloy Steels (AN-QQ-H-201).

6. C. G. Interrante, G. E. Hicho, and D. E. Harne, "A METALLURGICAL ANALYSIS OF ELEVEN STEEL PLATES TAKEN FROM A TANK CAR ACCIDNET NEAR CALLAO, MISSOURI", (Report No. 4), NBS Report 312.01/51, September 19, 1972.

7. C. Anderson, W. Townsend, J. Zook, and G. Cowgill, "THE EFFECTS OF A FIRE ENVIRONMENT ON A RAIL TANK CAR FILLED WITH LPG", B.R.L. Interim Memorandum Report No. 288, USA BAllistic Research Laboratories, Aberdeen Proving Ground, Maryland, September 1974.

Table I. Chemical Composition of Plate Samples from Insulated Tank Car RAX 202

Element	Specification AAR M128-69 Grade B	Chem. 1B (Shell Course 3)	Chem. 1C (Shell Course 3)	Chem. 3 (Shell Course 3)	Chem. 7 (Shell Course 4)	Chem. 11B (Shell Course 1)	Producers
	Ladle Analysis	Check Analysis[a]					Ladle Analysis[b]
	Percent By Weight						
Carbon	0.25 max.	0.24	0.24	0.24	0.23	0.24	0.23
Manganese	1.35 max.	1.32	1.31	1.26	1.32	1.25	1.33
Phosphorus	0.040 max.	0.006	0.007	0.007	0.006	0.005	0.007
Sulfur	0.050 max.	0.015	0.015	0.011	0.014	0.011	0.022
Silicon	0.30 max.	0.25	0.26	0.24	0.25	0.26	0.26
Vanadium	(c)	< 0.01	< 0.01	< 0.01	< 0.01	< 0.01	0.00
Copper	0.35 max.	0.22	0.22	0.21	0.21	0.21	(d)
Nickel	0.25 max.	0.19	0.19	0.19	0.19	0.19	(d)
Chromium	0.25 max.	0.11	0.11	0.11	0.11	0.11	(d)
Molybdenum	0.08 max.	0.06	0.06	0.06	0.06	0.06	(d)
Aluminum	(c)	0.030	0.030	0.035	0.030	0.030	(d)

(a) Carbon was determined by combustion - conductometric analysis; manganese, phosphorus, sulfur and molybdenum were determined by X-ray fluorescence analysis; silicon, nickel, chromium, copper, vanadium and aluminum were determined by emission spectroscopy.

(b) Producer's melt number for all plates used in tank car RAX 202 is C0485.

(c) Not specified.

(d) Not reported.

Table II. Macroscopic Observations of Plate Samples TC2-(1) and TC2-(3) From Shell Course 3

Plate Sample Identification	Fracture Surface Location	Fracture Mode	Presence of Secondary Crack	Plate Thinning, Percent
TC2-(1)	0	Shear, HAZ	No	2.5 (2) (a)
	1/2	Shear, HAZ	No	2.5 (2)
	3 1/2	Shear	No	20.2 (10)
	4	Stress-Rupture Mode	Yes	27.4 (7 1/2)
	5		Yes	37.8 (3 1/2)
	6		Yes	31.7 (3 1/2)
	7		Yes	26.4 (4)
	8		Yes	23.2 (3 1/2)
	9	Shear	No	19.8 (9)
	10	Shear	No	9.9 (3) (b)
	11	Shear, HAZ	No	6.2 (2)
	12	Shear, HAZ	No	3.1 (2)
TC2-(3)	13	Mixed, HAZ	No	8.6 (3 1/2)
	14	Mixed, HAZ	No	5.6 (2 1/2)
	15	Shear, HAZ	No	5.5 (1)
	16	Shear, HAZ	No	3.7 (1)

(a) Distance in inches from fracture surface to reach full plate thickness.

(b) Full plate thickness not reached, percent thinning calculated from position indicated.

Table III. Hardness Data Summary

Plate Identification	Hardness Measurement Location[a]		Average Rockwell B Hardness: As-Received Plate	Stress Relieved @ 1000°F 10 minutes	Stress Relieved @ 1160°F 15 minutes	Stress Relieved @ 1221°F 15 Minutes
SHELL COURSE 3						
TC2-(3) (Bottom of Tank Car)	Row 1		89 (26)[b]	88 1/2 (4)	88 (4)	86 1/2 (4)
	Row 3		88 (26)	88 (4)	88 (4)	87 (4)
	Row 5		89 1/2 (26)	89 (4)	87 1/2 (4)	87 (4)
		Average[c]	89	88 1/2	88	87
TC2-(1) (Near top of Tank Car)	Row 1		86 (20)			
	Row 3		87 (21)			
	Row 5		86 1/2 (21)			
		Average[c]	86 1/2			
			As-Received Plate	Stress Relieved @ 1118°F 15 minutes	Stress Relieved @ 1215°F 10 minutes	Stress Relieved @ 1257°F 15 minutes
SHELL COURSE 1						
TC2-(11B) (Bottom of Tank Car)	Row 1		90 (31)	90 (6)	90 (4)	89 (5)
	Row 3		86 1/2 (32)	87 (6)	86 (4)	85 (5)
	Row 5		90 (31)	90 (6)	89 (4)	88 1/2 (5)
		Average[c]	89	89	88 1/2	87 1/2
TC2-(10B) (Top of Tank car)	Row 1		89 1/2 (21)			
	Row 3		86 (21)			
	Row 5		89 (20)			
		Average[c]	88			

(a) See Figure 31 for identification.

(b) Number of hardness measurements taken.

(c) Average hardness values to nearest 1/2 R_B point.

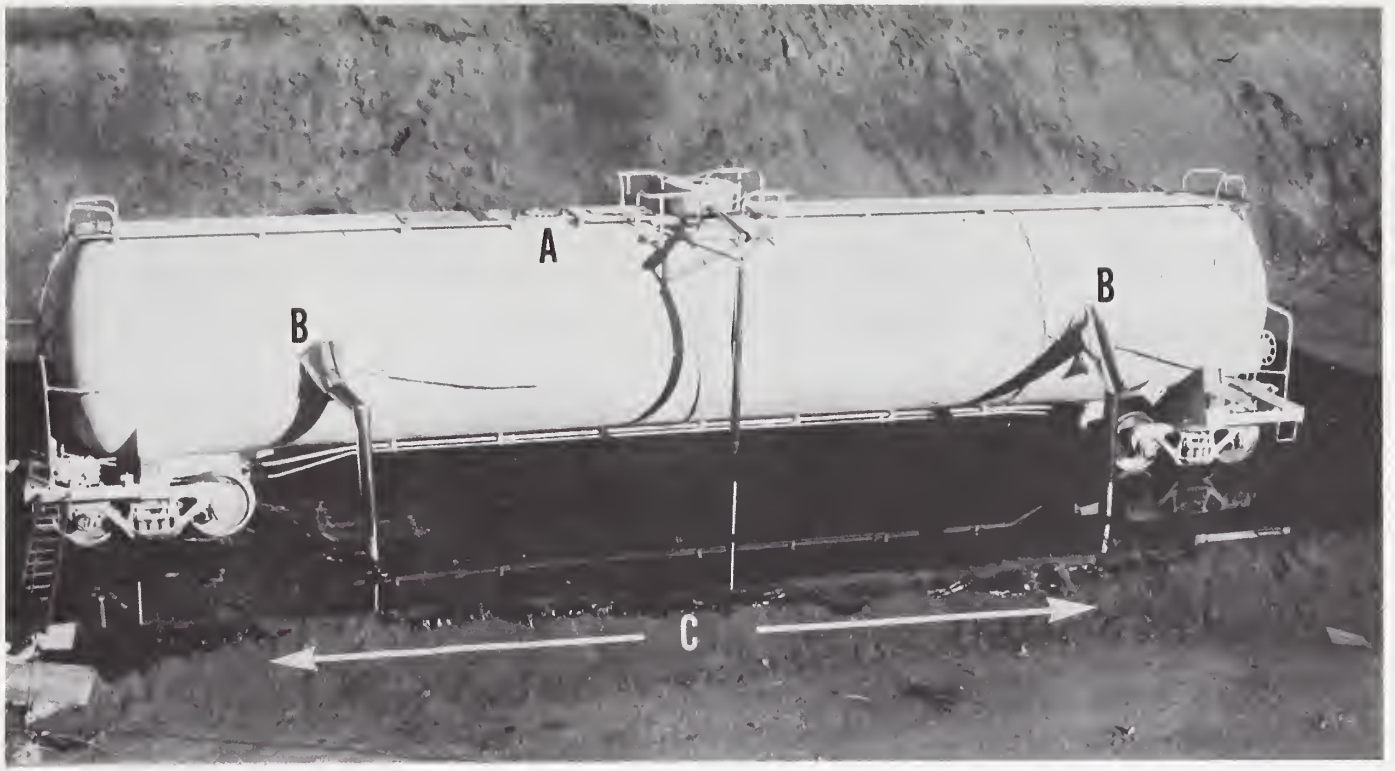

Figure 1. Insulated Tank Car RAX 202 Positioned in the Pit Prior to Initiation of the Fire Test.

The additional manway, shown at A, and the instrumentation cable ports, shown at B, are modifications of this standard 33,000 gallon tank car. The JP-4 fuel dike is shown at C. Mag. X 1/84

a

Figure 2. Photographs of Fragments of Tank Car RAX 202 After Failure.

a. Fragment A contains the A-head plate and shell courses 1 and 2. Fragment B contains the B-head plate and shell courses 4, 5, 6, and 7.

b. Largest fragment of shell course 3, Fragment C, showing additional manway.

c. Smallest fragment of shell course 3, Fragment D.

Original color photographs courtesy U.S. Army.

b

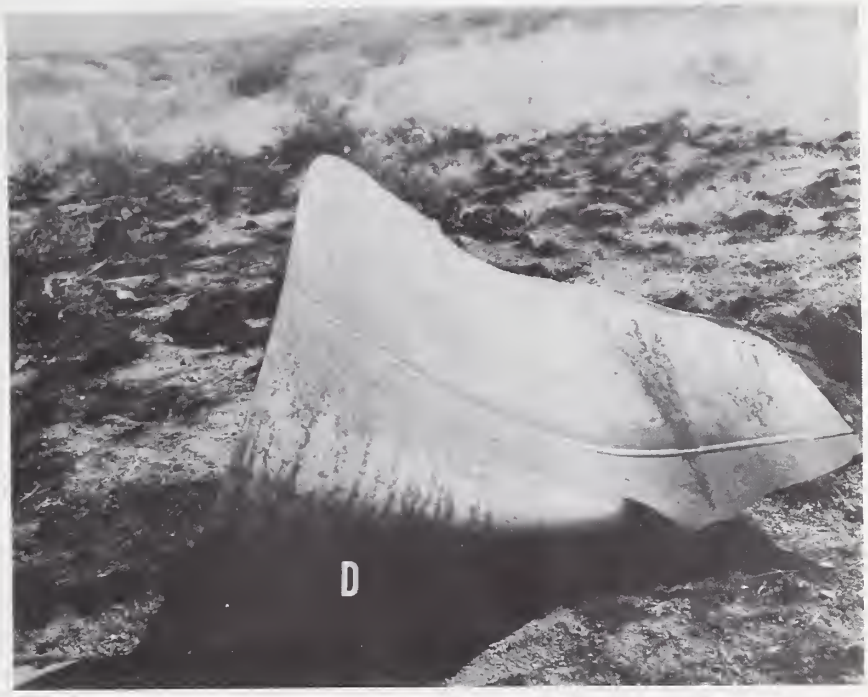

c

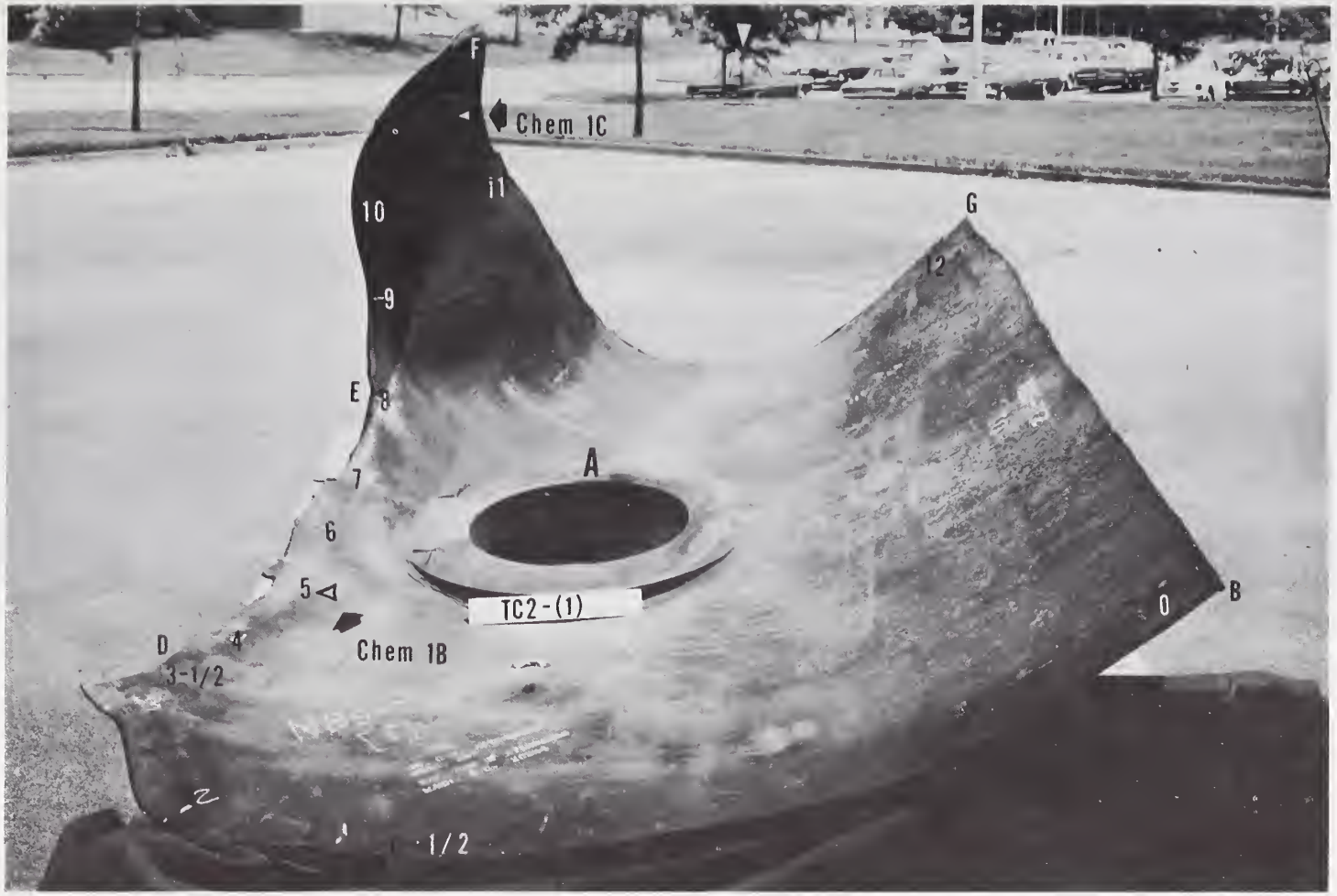

Figure 3. Plate Sample TC2-(1), Shell Course 3, Taken from Fragment C.

Photograph shows the inside plate surface at the top of the tank car with the additional manway shown at A. Line BCDEFG is the fracture surface. Line BC adjoins the girth weld connecting shell course 3 to shell course 4, and line FG adjoins the girth weld connecting shell course 3 to shell course 2. Thickness measurements were made at locations 0,1/2,3-1/2,4,5,6,7,8,9,10, 11, and 12. Specimens for chemical analysis were taken from areas marked Chem. 1B and Chem. 1C. Mag. X 1/12

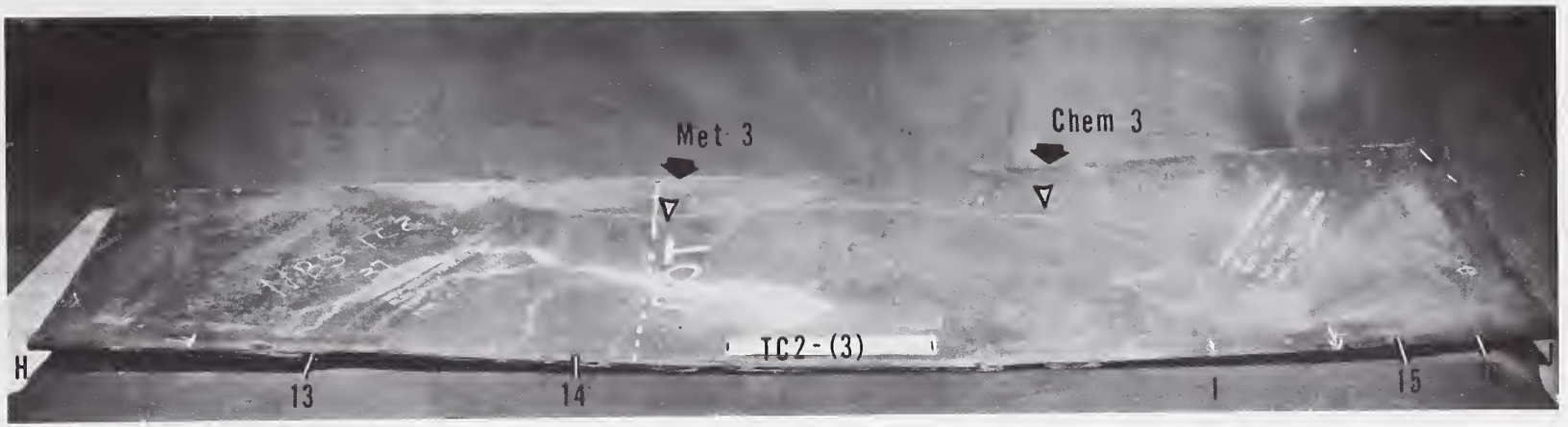

Figure 4. Plate Sample TC2-(3), Shell Course 3, Taken from Fragment C.

Photograph shows the inside plate surface with the bottom of the tank car marked BOT. Line HIJ is the fracture surface. Specimens for metallographic examination and chemical analysis were taken from areas marked Met. 3 and Chem. 3, respectively. Thickness measurements were made at locations 13, 14,15, and 16. Mag. X 1/12

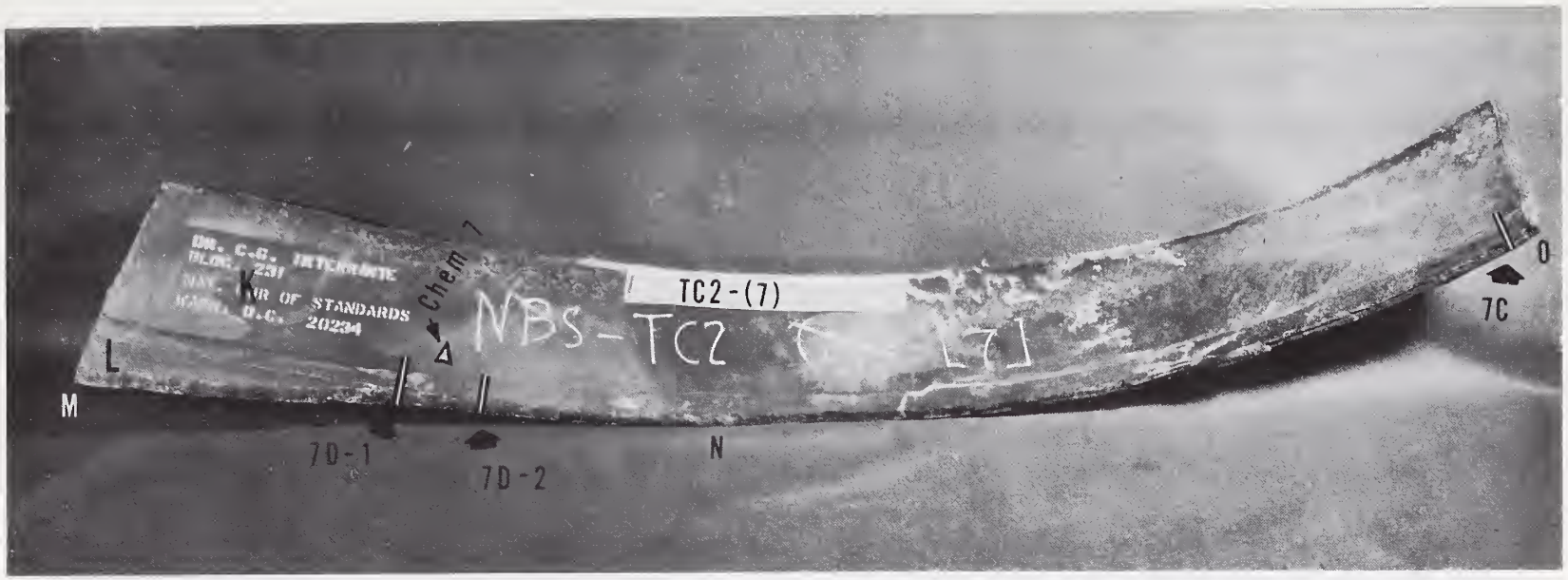

Figure 5. Plate Sample TC2-(7), Shell Course 4, Taken from Fragment B.

Photograph shows the inside plate surface of shell course 4, marked K, with a small piece of shell course 3, marked L, connected by a portion of a girth weld. Line MNO is the fracture surface. Specimens for metallographic examination were taken from areas marked 7C,7D-1, and 7D-2, and a specimen for chemical analysis was taken from the area marked Chem. 7. Mag. X 1/8

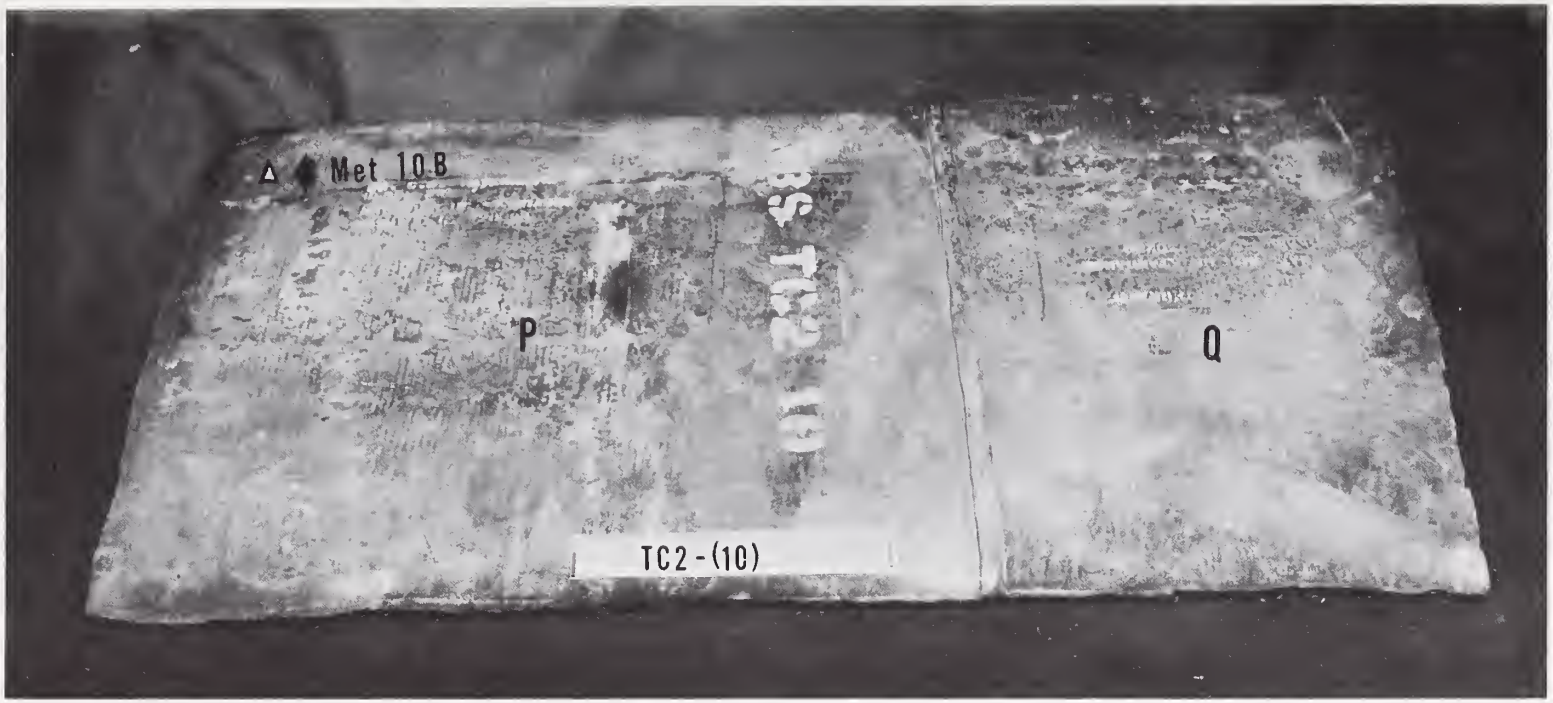

Figure 6. Plate Sample TC2-(10) Taken from Shell Courses 1 and 2 of Fragment A at the Top of the Tank Car.

Photograph shows the outside plate surface of shell course 1 (TC2-(10B)), marked P, and shell course 2 (TC2-(10A)), marked Q. Specimen for metallographic examination was taken from the area marked Met. 10B. Mag. X 1/7

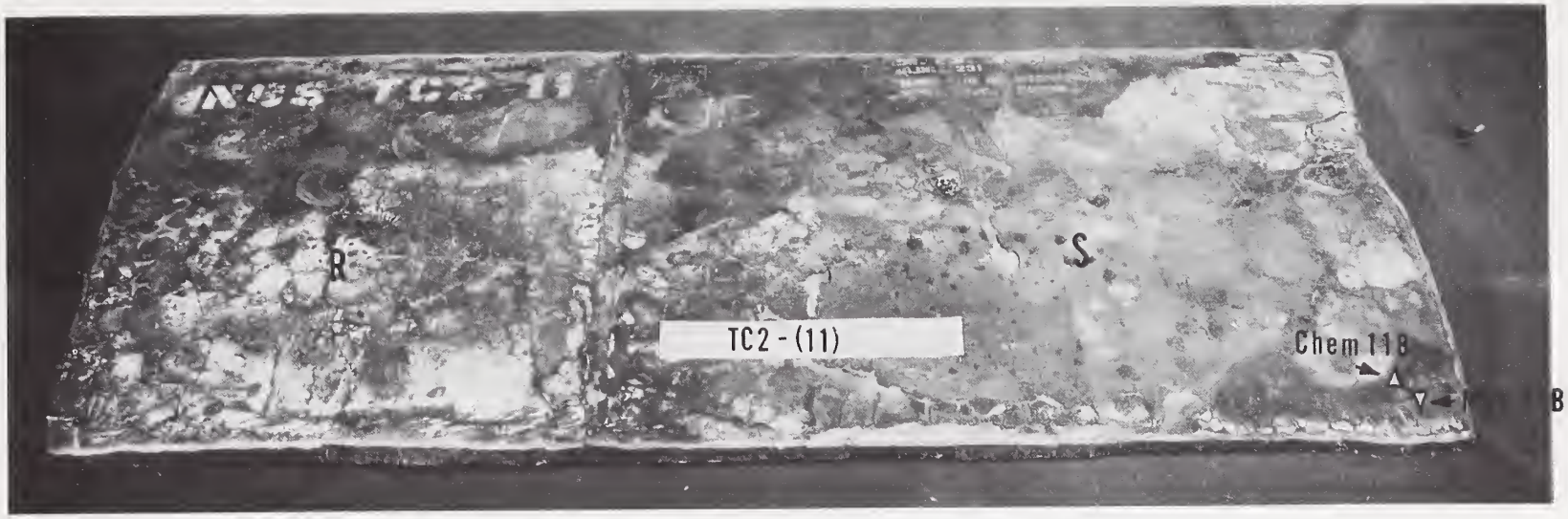

Figure 7. Plate Sample TC2-(11) Taken from Shell Courses 1 and 2 of Fragment A at the Bottom of the Tank Car.

Photograph shows the outside plate surface of shell course 1 (TC2-(11B)), marked S, and shell course 2 (TC2-(11A)), marked R. Specimens for metallographic examination and chemical analysis were taken from areas marked Met. 11B and Chem. 11B, respectively. Mag. X 1/8

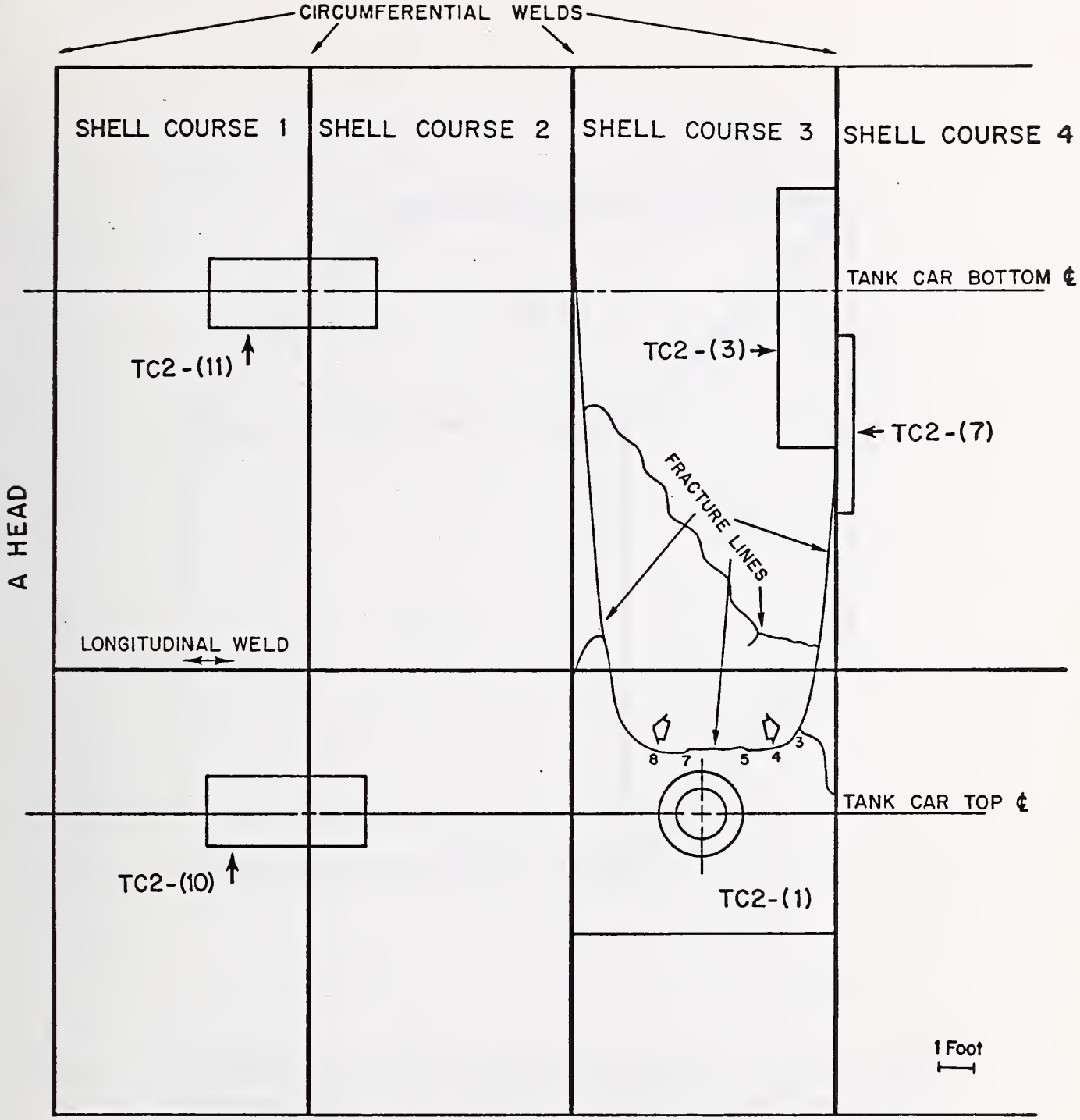

Figure 8. Schematic Diagram Showing the Location of NBS Samples in Tank Car RAX 202, Viewed from the Outside of the Tank Car. The direction of crack propagation is indicated by the open arrows ⇩.

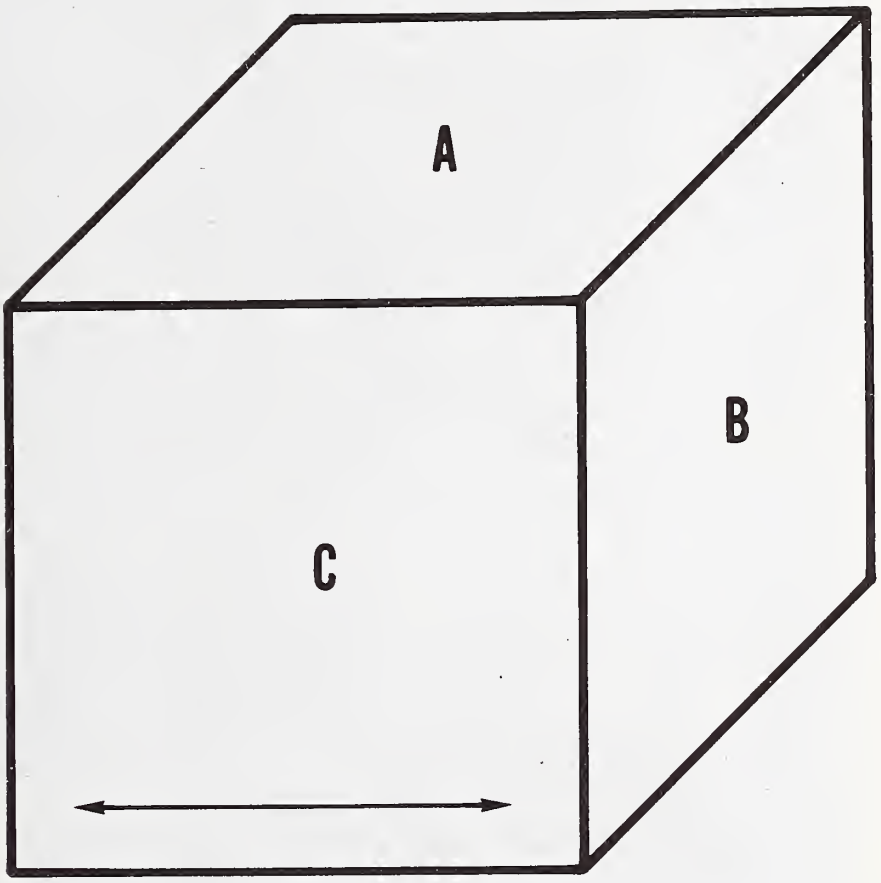

Figure 9. Schematic Showing the Three Mutually Perpendicular Planes Associated with the Rolling Direction in a Steel Plate.

Plane A is perpendicular to the short transverse direction and is parallel to the plate surface. Plane B is a transverse plane perpendicular to the rolling direction, and plane C is a longitudinal plane, perpendicular to the surface, parallel to the rolling direction. The arrow shown on the C plane indicates the rolling direction.

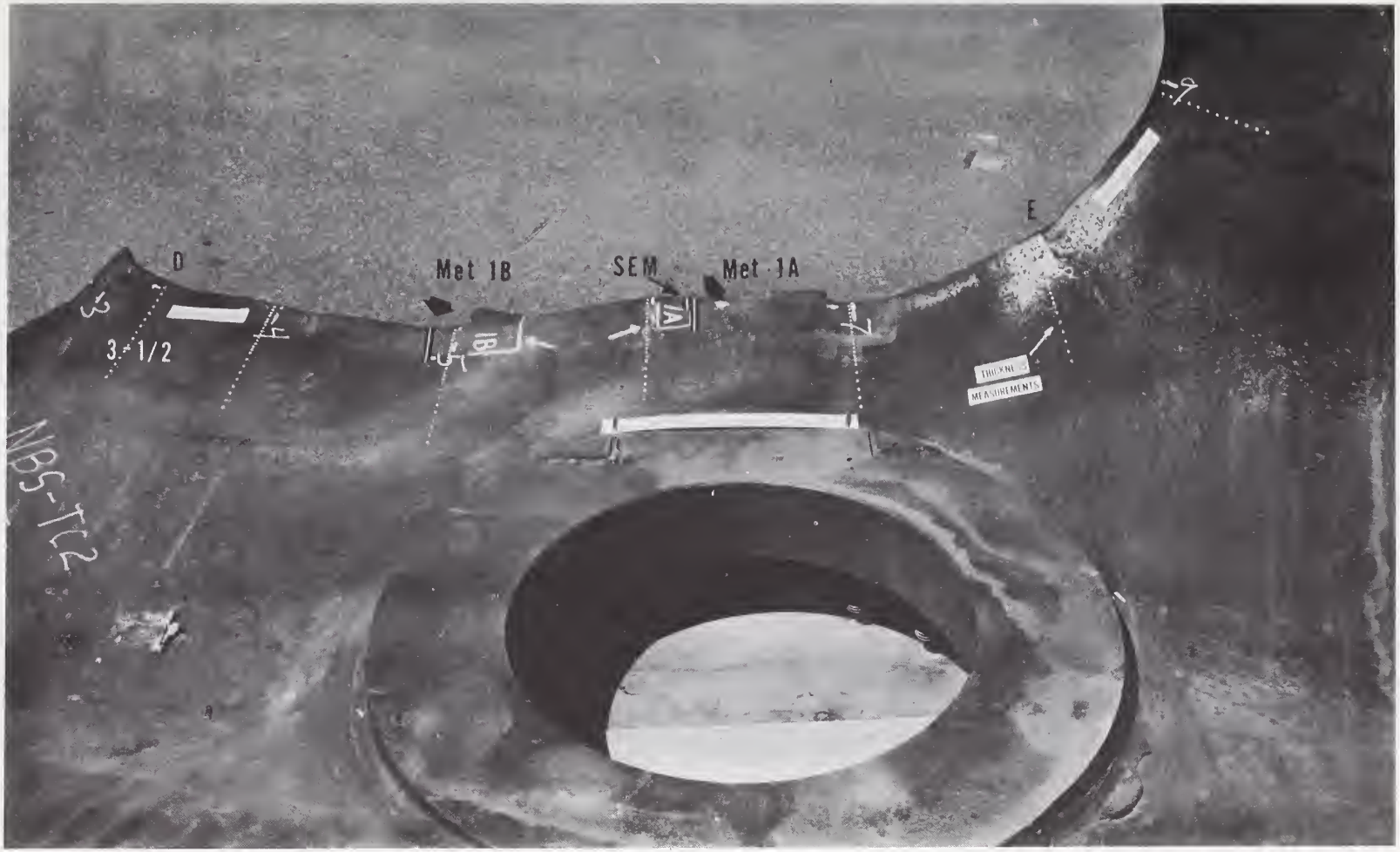

Figure 10. Close-up of a Portion of the Inside Surface of Plate Sample TC2-(1).

Line DE is the location along which the fracture was initiated. Specimens for metallographic examination were taken from areas marked Met. 1A and Met. 1B. A portion of the fracture surface, marked SEM, was removed for examination by scanning electron microscopy. Mag. X 1/7

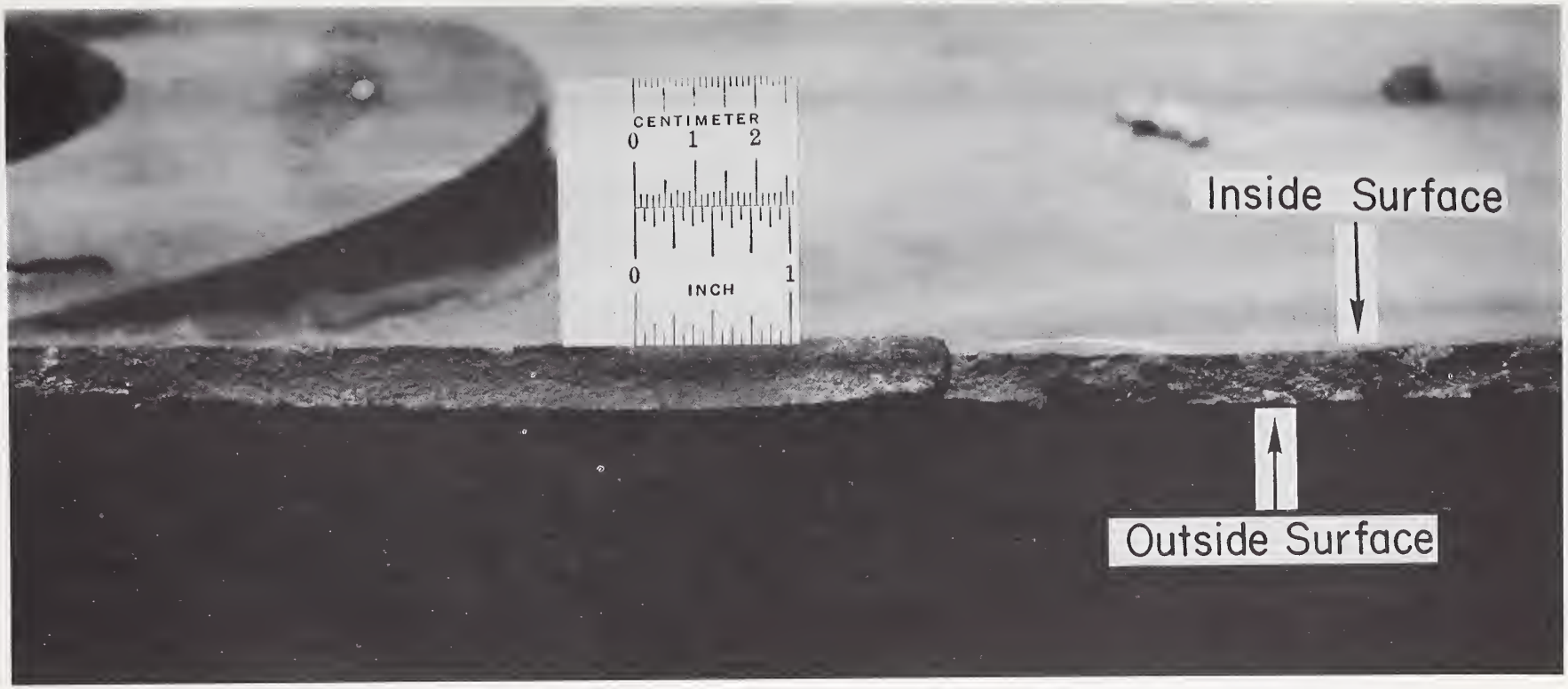

Figure 11. Macrograph of Fracture Face of TC2-(1) Between Locations 5 and 6.

The fracture face is nearly perpendicular to the plate surface with evidence of very small shear lips at both the inside and outside plate surface. Mag. X 0.9

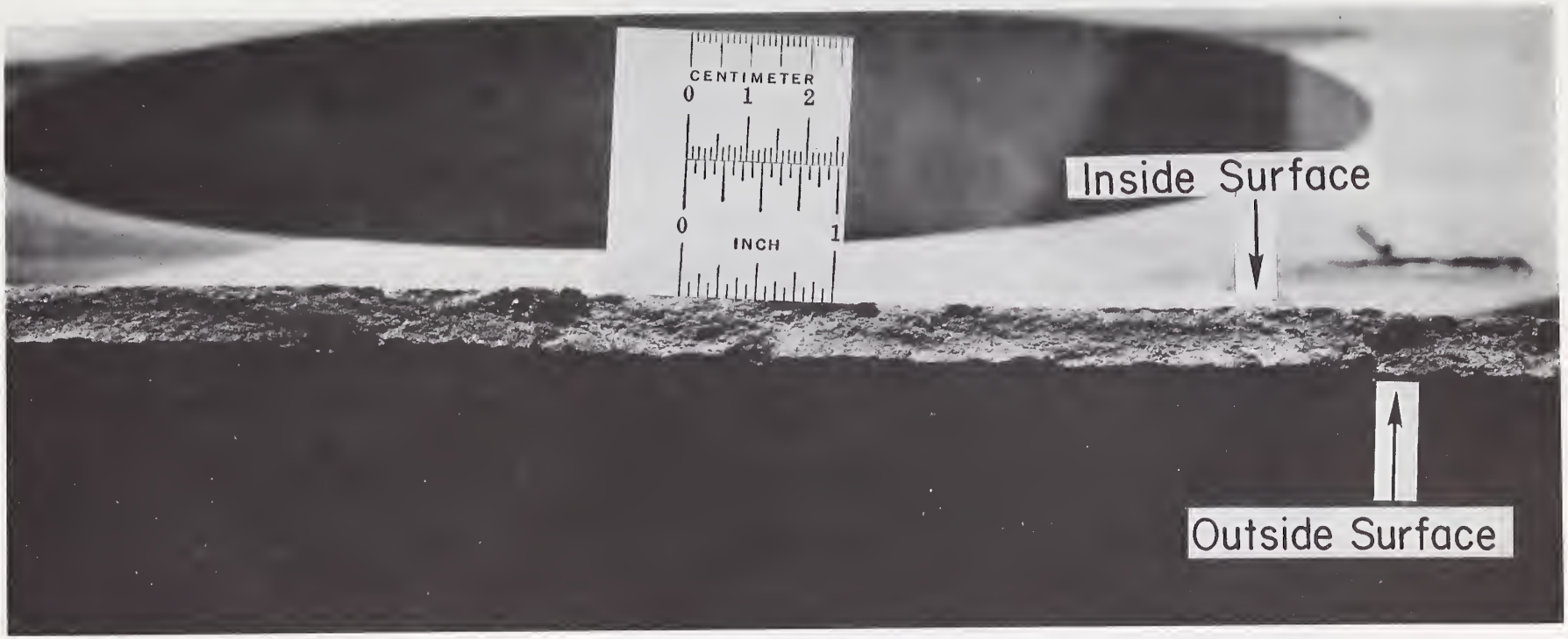

Figure 12. Macrograph of Fracture Face of TC2-(1) Between Locations 6 and 7.

The fracture face is nearly perpendicular to the plate surface with evidence of very small shear lips at both the inside and outside plate surface. Mag. X 0.9

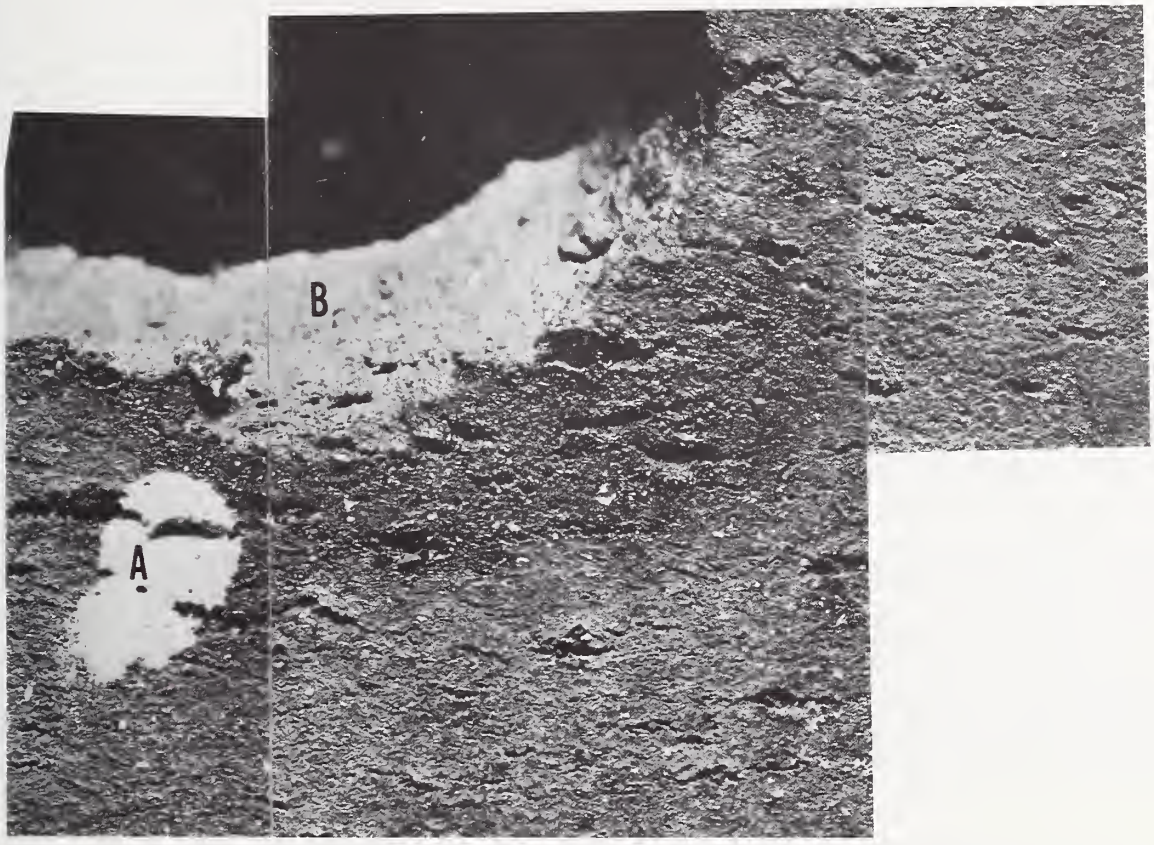

Figure 13. Macrograph of Inside Plate Surface of TC2-(1) at the Fracture Surface.

Photograph was taken near location 5 and shows numerous secondary surface cracks. A spot of white marking paint is shown at A and a portion of the fracture surface is shown at B. Mag. X 5

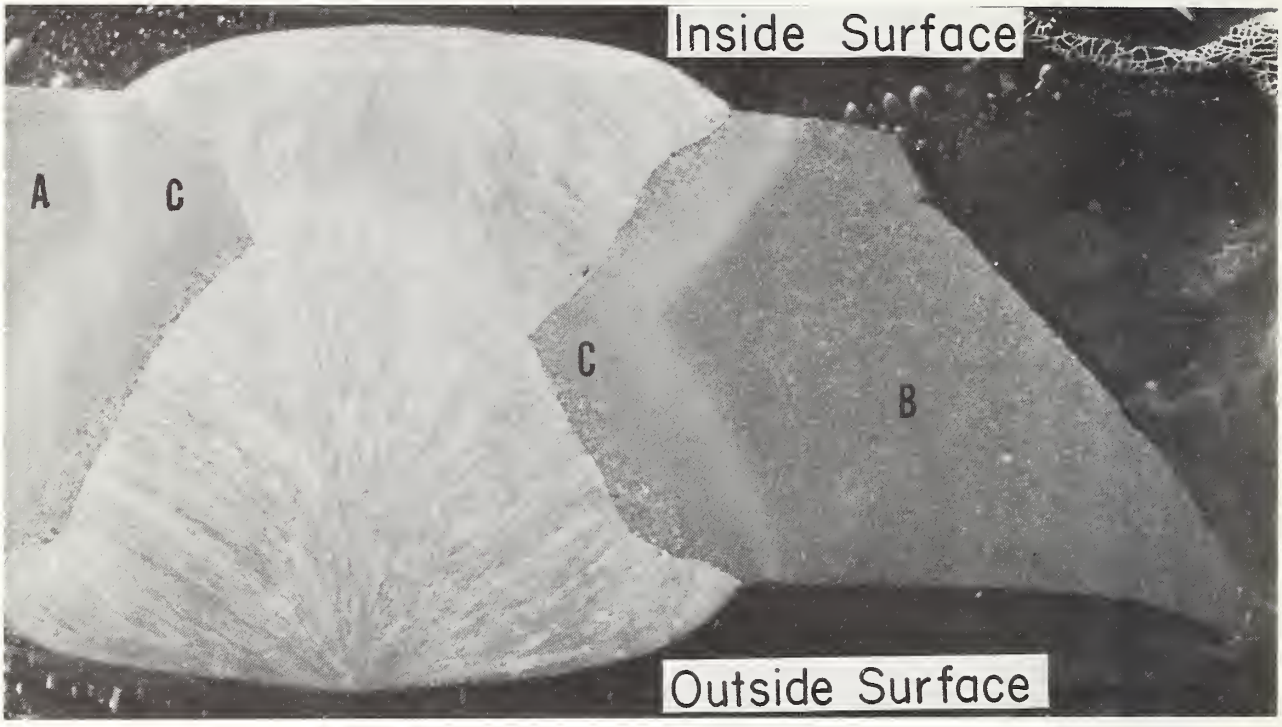

a

Figure 14. Profile Views of Fracture Surface on Plate Sample TC2-(7).

A is shell course 4, B is shell course 3, and C is the weld HAZ.

a. Location 7D-1, shear failure at 45° to the plate surface.
b. Location 7D-2, shear failure at 45° to the place surface in weld HAZ.
c. Location 7C, mixed mode fracture in weld HAZ with a nearly perpendicular region (N.P.) bounded by two shear failure regions.

Etch: 5% Nital. Mag. X 4

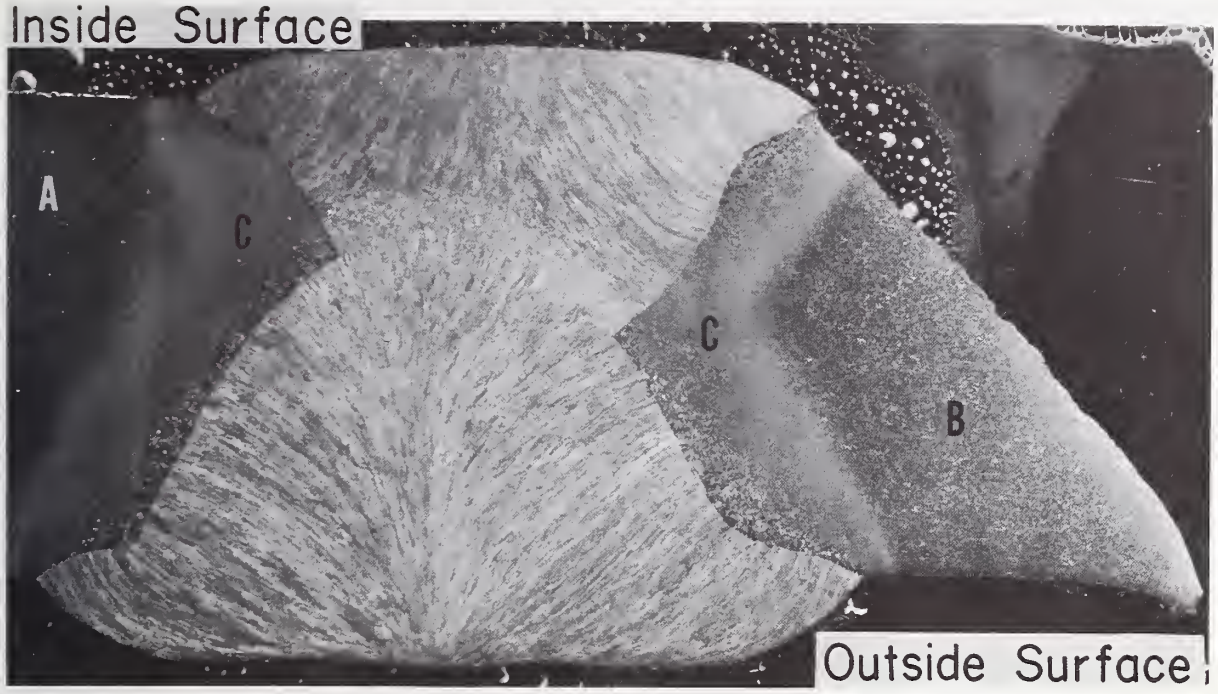
Inside Surface
A
C
C
B
Outside Surface

b

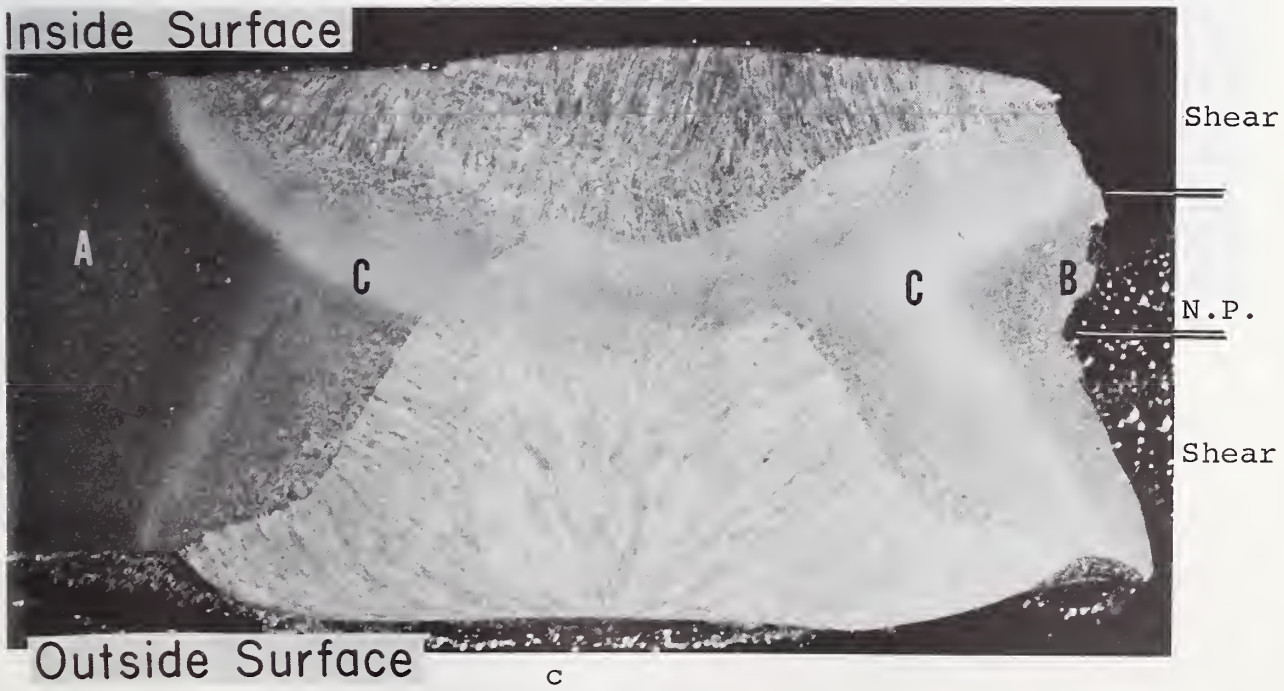
Inside Surface
A
C
C
B
Shear
N.P.
Shear
Outside Surface

c

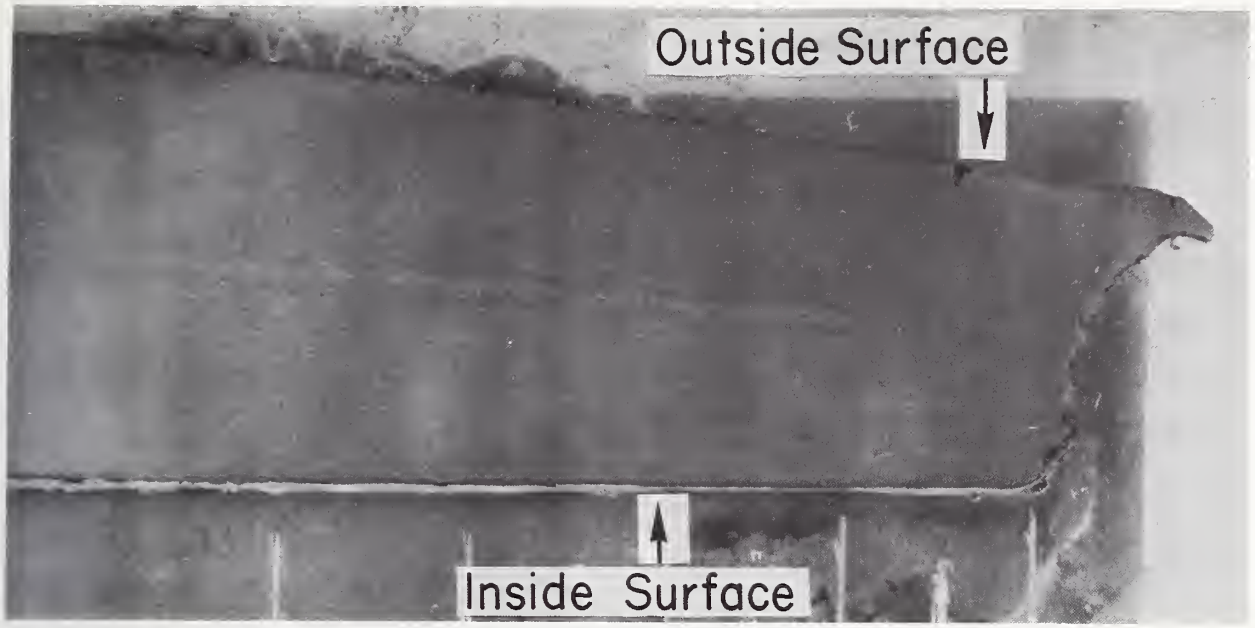

a

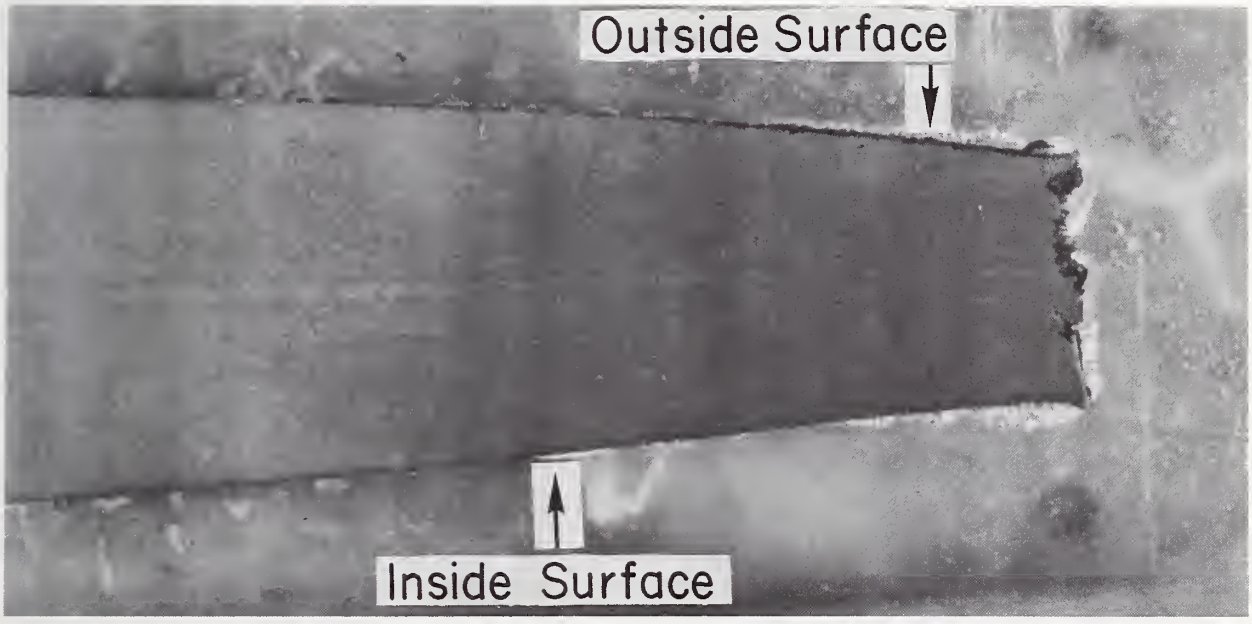

b

Figure 15. Profile Views of Fracture Surface on Plate Sample TC2-(1), Shell Course 3.

Fracture surface is nearly perpendicular to plate surfaces with evidence of very small shear lips at the plate surfaces.

a. Location 6
b. Location 5

Etch: 5% Nital. Mag. X 4

Figure 16. Representative Microstructures of Plate Sample TC2-(1) Away from Fracture Face. AAR TC128-B-69 Steel.

Micrographs taken on the C plane of shell course 3 near the top of the tank car showing moderate banding at the plate midthickness position. Ferrite grain size number 8-1/2.

Etch: 5% Nital. Mag. X 100

Outside Surface

Midthickness Region

Inside Surface

Figure 17. Representative Microstructures of Plate Sample TC2-(3). AAR TC128-B-69 steel.

Micrographs taken on the C plane of shell course 3 at the bottom of the tank car showing moderate banding at the plate midthickness position. Ferrite grain size number 8-1/2.

Etch: 5% Nital. Mag. X 100

Outside Surface

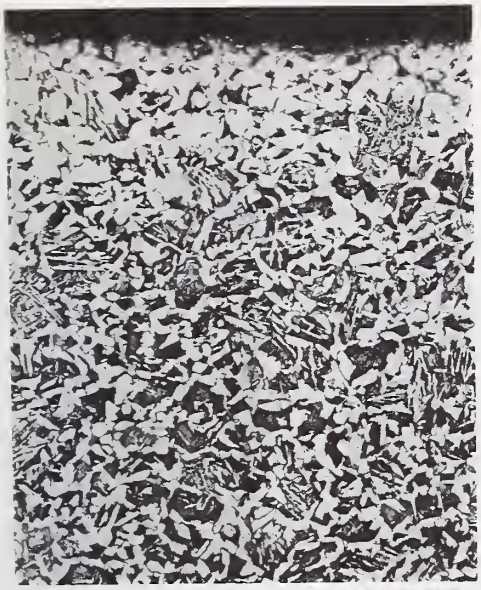

Midthickness Region

Inside Surface

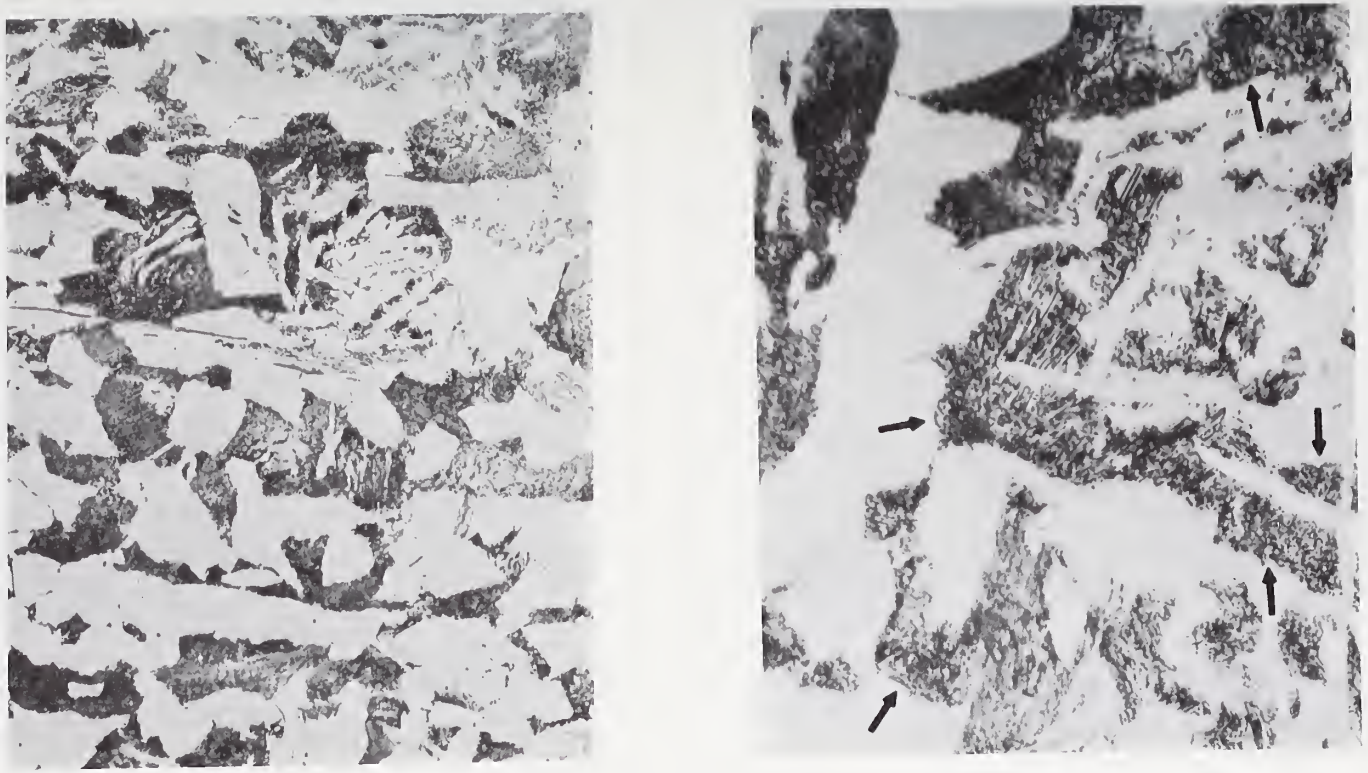

a b

Figure 18. Photomicrographs of Plate Sample TC2-(1) Adjacent to Hardness Specimens.

a. C plane, near outside plate surface showing that the lamellar pearlite is not resolved. Mag. X 500

b. C plane, near outside plate surface with arrows indicating some of the spheroidized iron carbide regions. Mag. X 1250

Etch: 4% Picral.

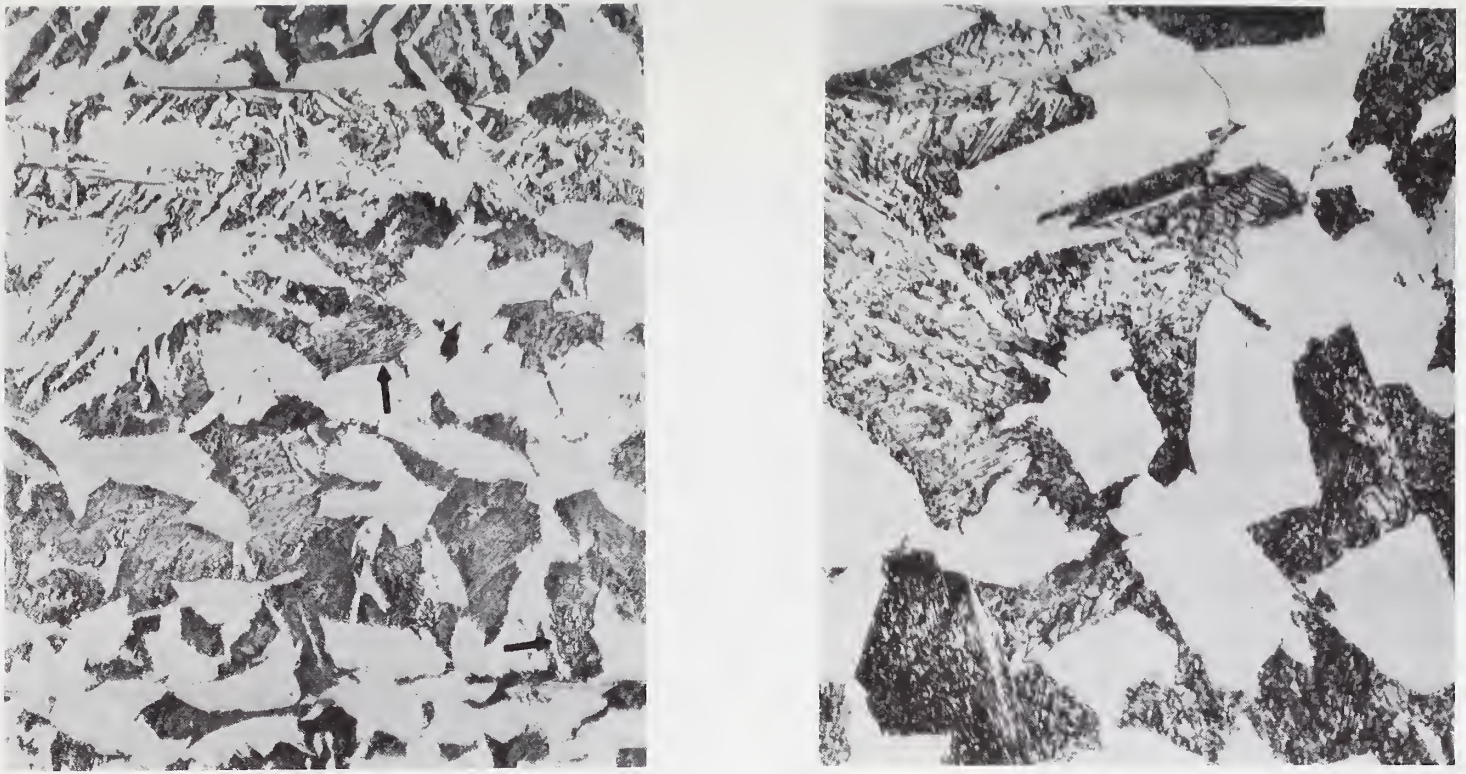

a b

Figure 19. Photomicrographs of Plate Sample TC2-(3) Adjacent to Hardness Specimens.

a. C plane, near midthickness position, arrows indicate resolved lamellar pearlite regions. Mag. X 500

b. C plane, near outside plate surface, showing strong lamellar character of the pearlite. Mag. X 1250

Etch: 4% Picral.

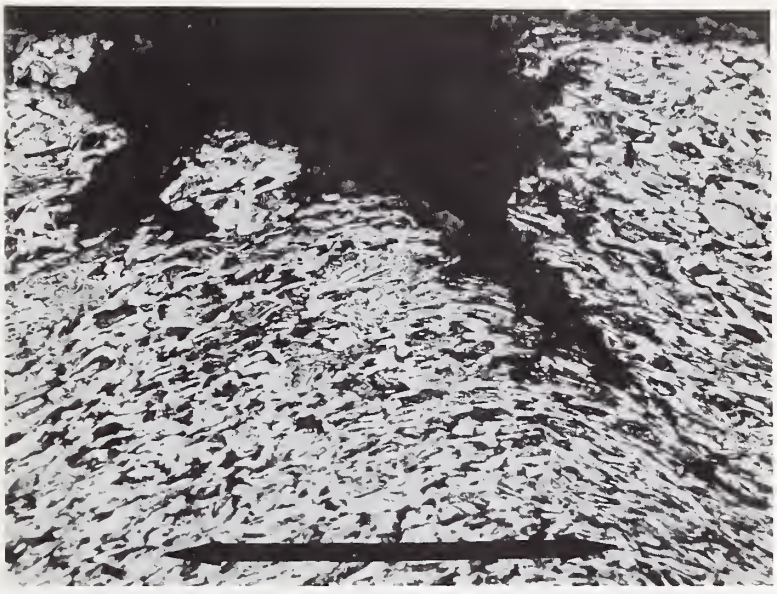

a

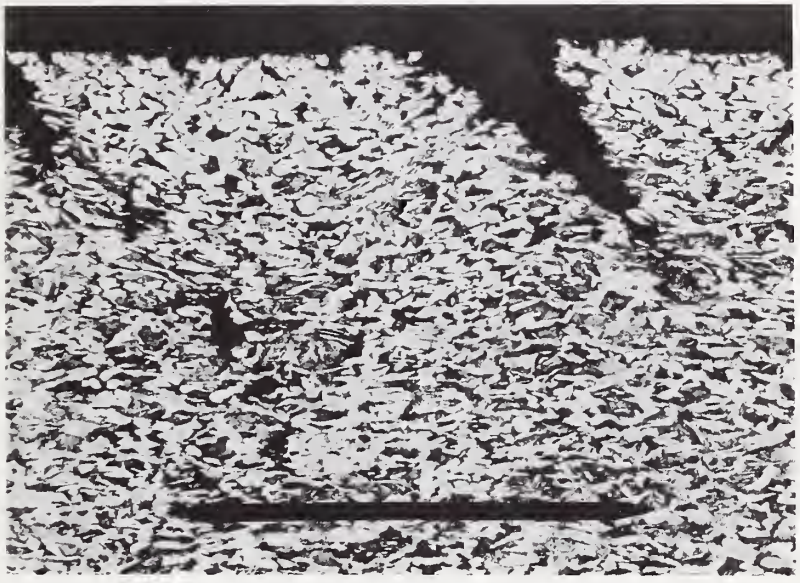

b

Figure 20. Photomicrographs of the Plate Surface of Plate Sample TC2-(1) near the Fracture Surface Showing Extensive Deformation of the Ferrite Grains.

Arrows indicate the direction of the principal or hoop stress.

a. C plane, outside plate surface.

b. C plane, inside plate surface.

Etch: 5% Nital. Mag. X 100

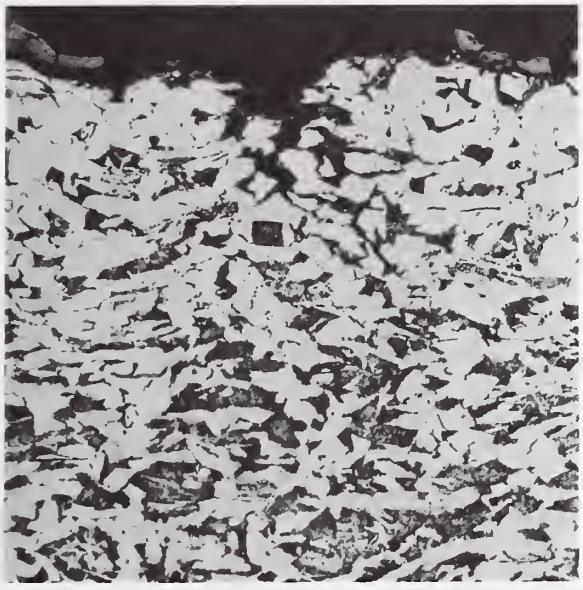

a

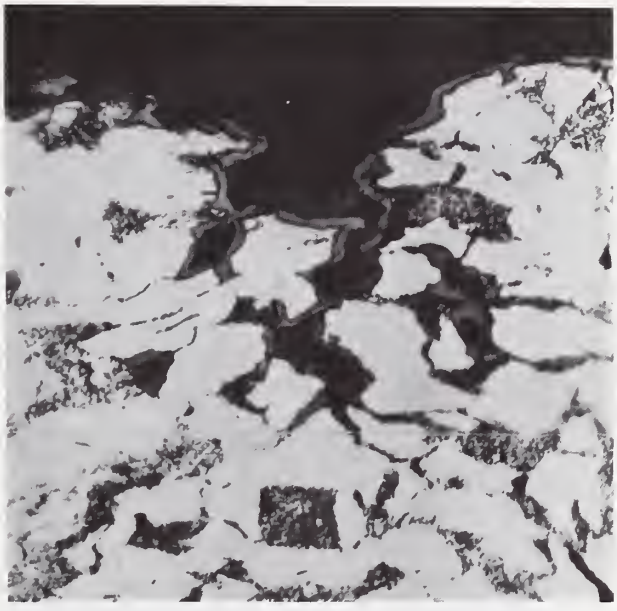

b

Figure 21. Photomicrograph of an Intergranular Crack Near the Fracture Initiation Site on Plate Sample TC2-(1).

a. C plane. Mag. X 200

b. C plane. Mag. X 500

The gray layer on the inside plate surface, crack surfaces, and voids near the surface is believed to be iron oxide.

Etch: 4% Picral.

a

b

Figure 22. Photomicrographs of Fracture Surface of Plate Sample TC2-(1) Showing the Profile of the Fracture Edge, the Elongated Ferrite Grains and Cracks Near the Fracture Edge.

a. C plane, near outside plate surface

b. C plane, near inside plate surface

Etch: 5% Nital. Mag. X 100

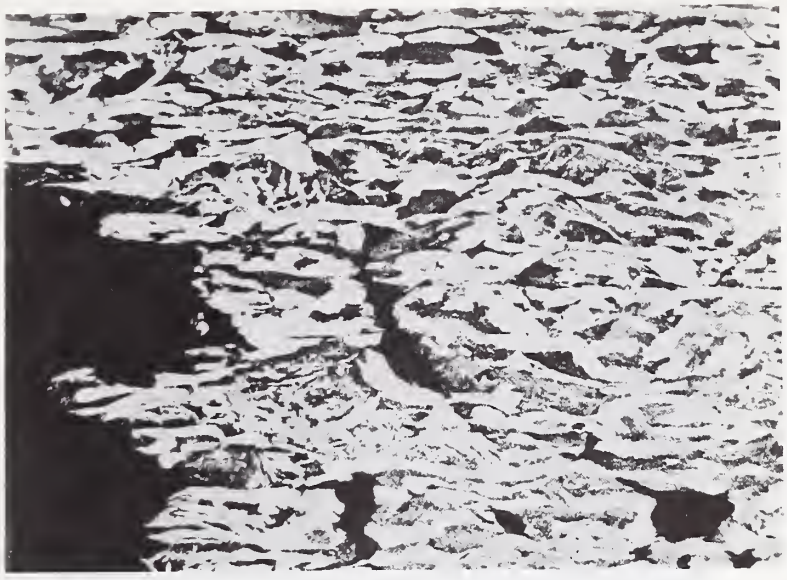

a

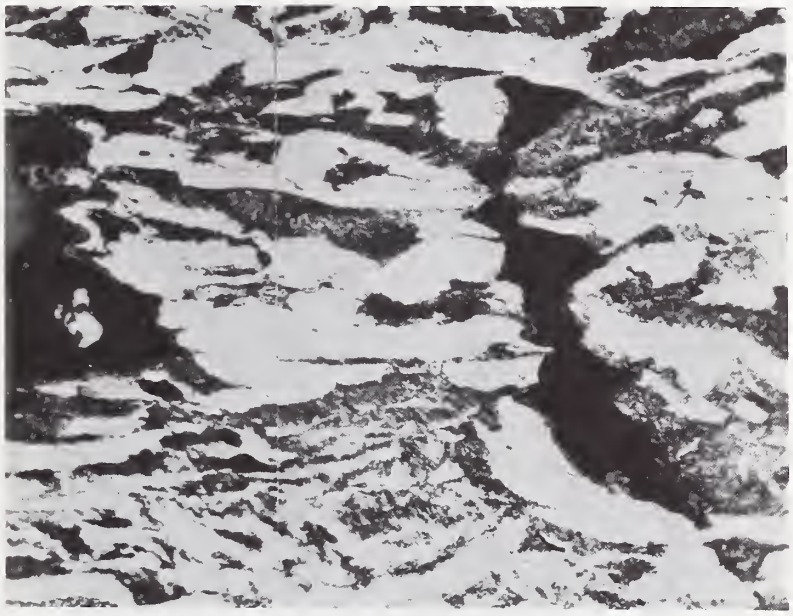

b

Figure 23. Photomicrographs of the Fracture Surface and the Regional Immediately Behind the Fracture Surface on Plate Sample TC2-(1).

a. C plane. Mag. X 200

b. C plane. Mag. X 500

The gray layer on the fracture surface and crack surface is believed to be iron oxide.

Etch: 4% Picral.

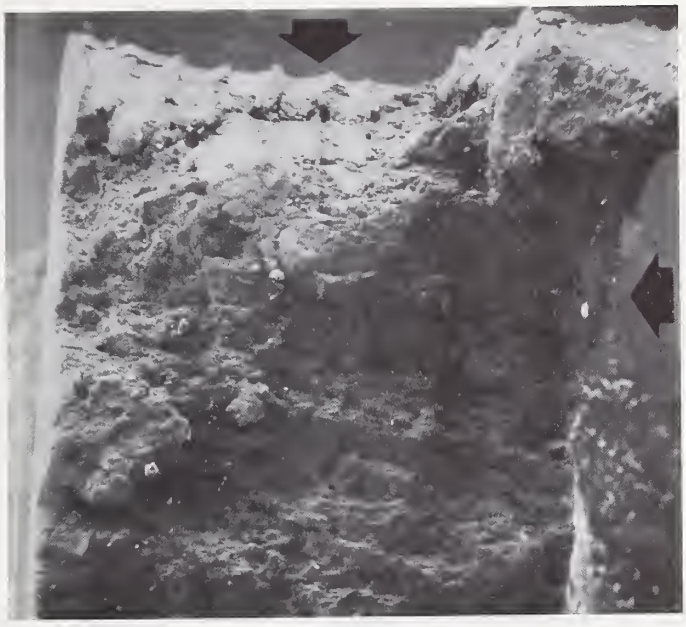

a

b

Figure 24. SEM Fractographs of the Fracture Surface of Plate Sample TC2-(1) in the Fracture Inition Region Near the Outside Plate Surface.

a. Outside plate surface at the top of the photograph, near location 6. Mag. X 14

b. Higher magnification photograph of the region indicated by the arrows in (a). Mag. X 190

a

b

Figure 25. SEM Fractographs of Fracture Surface of Plate Sample TC2-(1) in the Fracture Initiation Region Near the Plate Midthickness Region.

a. Near location 6. Mag. X 13

b. Higher magnification photograph of the region indicated by the arrows in (a). Mag. X 190

a

Figure 26. SEM Fractographs of the Fracture Surface of Plate Sample TC2-(1) in the Fracture Initiation Region Near the Inside Plate Surface.

a. Inside plate surface at the bottom of the photograph, near location 6. Mag. X 13

b. Higher magnification photograph of the region indicated by arrows in (a). Mag. X 100

c. Higher magnification photograph of the region indicated by arrows in (b). Mag. X 190

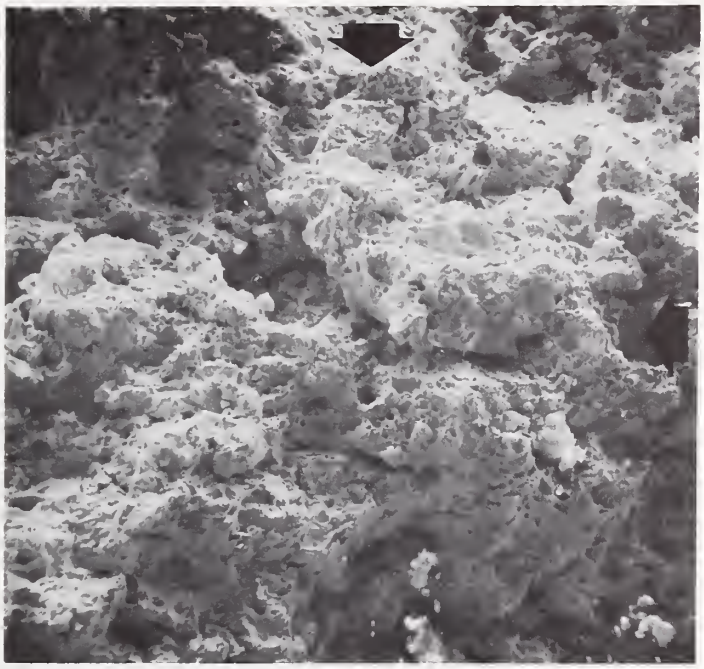

b

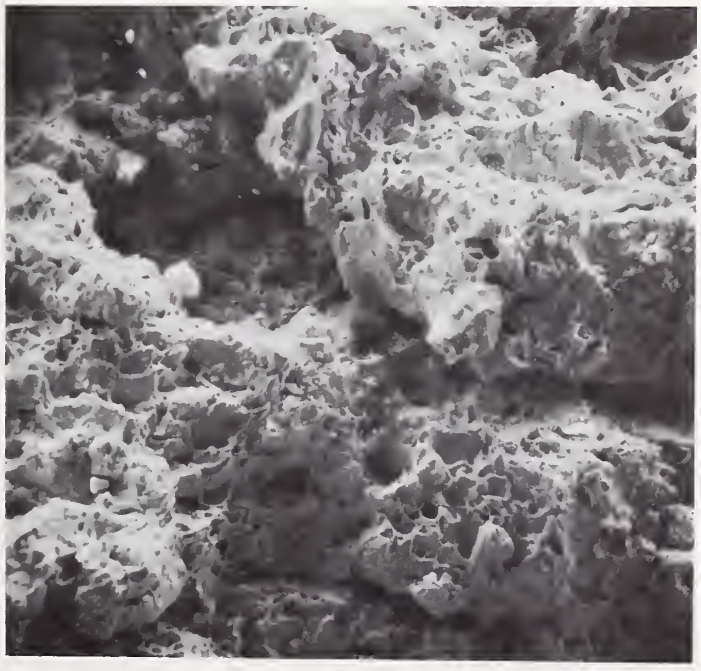

c

Figure 27. Representative Microstructures of Plate Sample TC2-(10B). AAR TC128-B-69 Steel.

Micrographs taken on the C plane of shell course 1 at the top of the tank car showing moderate banding at the plate midthickness position. Ferrite grain size number 8.

Etch: 5% Nital. Mag. X 100

Outside Surface

Midthickness Region

Inside Surface

Figure 28. Representative Microstructures of Plate Sample TC2-(11B). AAR TC128-B-69 Steel.

Micrographs taken on the C plane of shell course 1 at the bottom of the tank car showing moderate banding at the plate midthickness position. Ferrite grain size number 8-1/2.

Etch: 5% Nital. Mag. X 100

Outside Surface

Midthickness Region

Inside Surface

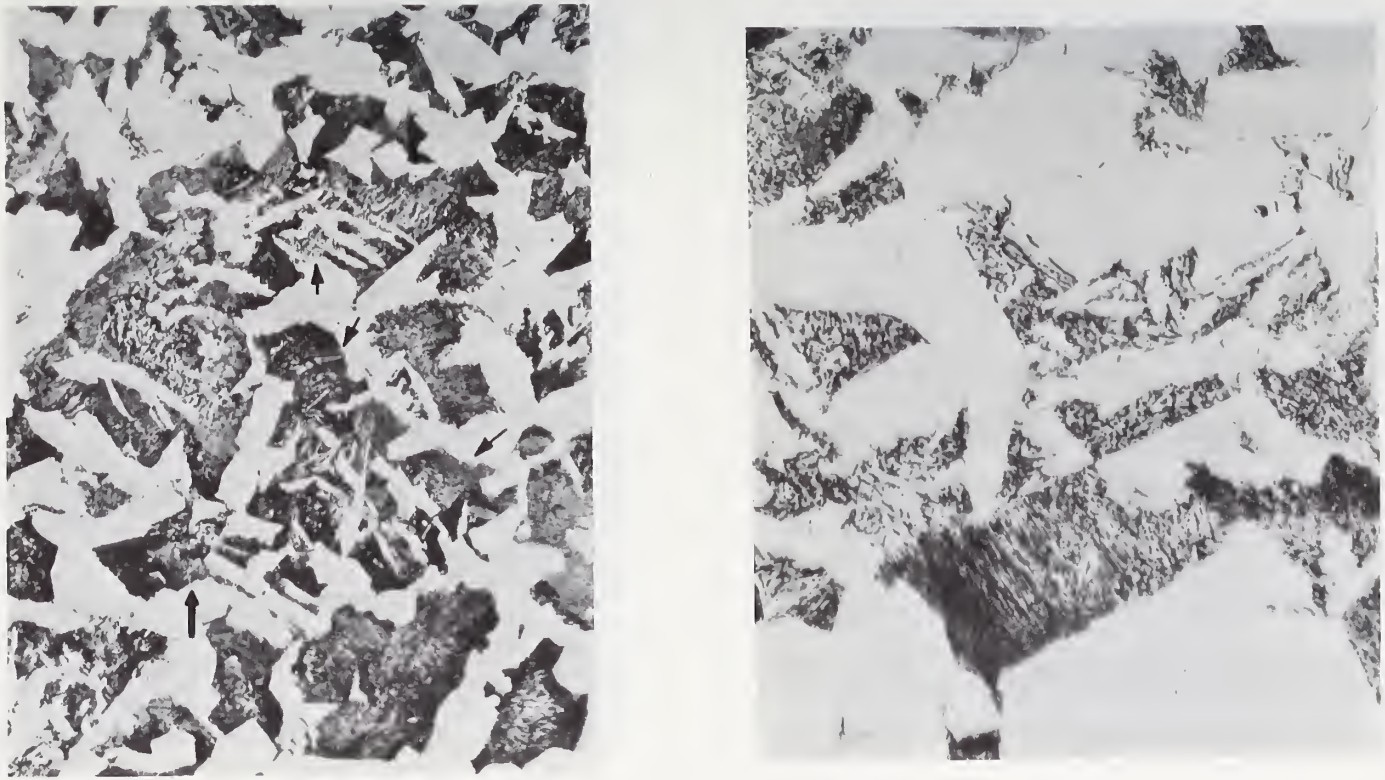

a b

Figure 29. Photomicrographs of Plate Sample TC2-(10B) Adjacent to Hardness Specimens.

a. C plane, near inside plate surface, arrows indicate resolved lamellar pearlite regions. Mag. X 500

b. C plane, near midthickness position, showing strong lamellar character of the pearlite. Mag. X 1250

Etch: 4% Picral.

a b

Figure 30. Photomicrographs of Plate Sample TC2-(11B) Adjacent to Hardness Specimens.

a. C plane, near midthickness position, arrows indicate resolved lamellar pearlite regions. Mag. X 500

b. C plane, near midthickness position, showing strong lamellar character of the pearlite. Mag. X 1250

Etch: 4% Picral.

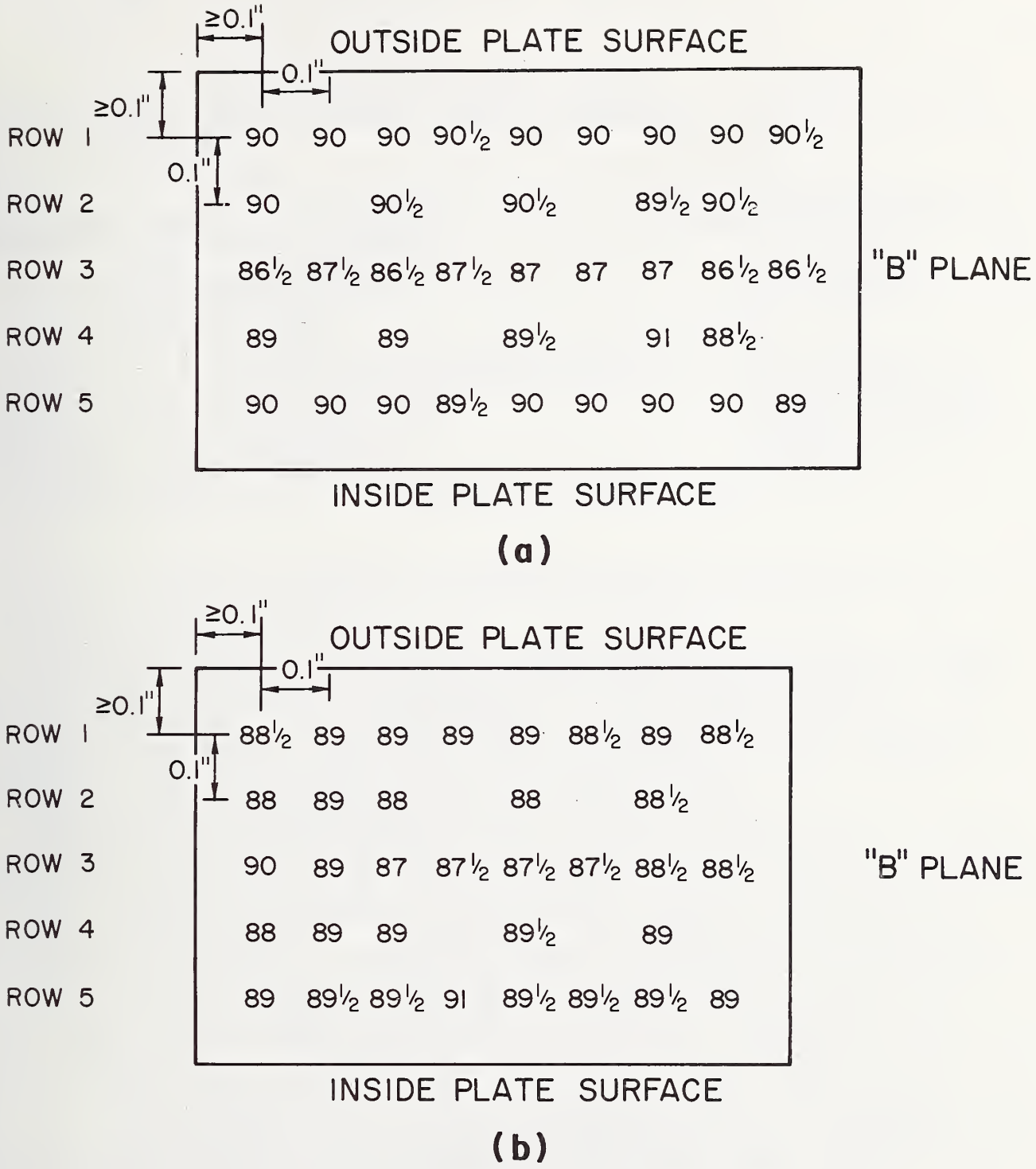

Figure 31. Schematic of Representative Hardness Profiles from Plate Samples TC2-(3) and TC2-(11B).

a. Specimen from TC2-(11B), B plane, as received.

b. Specimen from TC2-(3), B plane, as-received.

NBS-114A (REV. 7-73)

U.S. DEPT. OF COMM. BIBLIOGRAPHIC DATA SHEET	1. PUBLICATION OR REPORT NO. NBS IR 75-657	2. Gov't Accession No.	3. Recipient's Accession No.

4. TITLE AND SUBTITLE

Report No. 7 .

A METALLURGICAL INVESTIGATION OF A FULL-SCALE INSULATED RAIL TANK CAR FILLED WITH LPG SUBJECTED TO A FIRE ENVIRONMENT

5. Publication Date: January, 1975

6. Performing Organization Code:

7. AUTHOR(S): J. G. Early and C. G. Interrante

8. Performing Organ. Report No.: NBS IR 75-657

9. PERFORMING ORGANIZATION NAME AND ADDRESS

NATIONAL BUREAU OF STANDARDS
DEPARTMENT OF COMMERCE
WASHINGTON, D.C. 20234

10. Project/Task Work Unit No.: 3120413

11. Contract/Grant No.:

12. Sponsoring Organization Name and Complete Address (Street, City, State, ZIP)

Federal Railroad Administration
Department of Transportation
Washington, D. C. 20591

13. Type of Report & Period Covered: Failure Analysis Report

14. Sponsoring Agency Code:

15. SUPPLEMENTARY NOTES

16. ABSTRACT (A 200-word or less factual summary of most significant information. If document includes a significant bibliography or literature survey, mention it here.)

An analysis of the failure of an insulated rail tank car, RAX 202, which had been tested to failure in a fire environment at White Sands Missile Range, New Mexico, was requested by the Federal Railroad Administration, Department of Transportation. The tank car, filled with liquified petroleum gas (LPG), failed after approximately 94 minutes of exposure to a JP-4 jet fuel fire. Five plate samples were selected for laboratory study at the National Bureau of Standards.

The results of metallurgical investigations suggest that a region approximately 30 inches in length near the top of the tank car in shell course 3 was the site of the initial rupture of the tank car. The results of stress-relieving experiments conducted on samples taken from the top and bottom of the car indicated that the top of the tank car experienced temperatures of 1200°F to 1250°F for times of between 10 to 15 minutes.

The fracture features of the initial rupture were indicative of failure by a stress-rupture mechanism. It was concluded that this 30-inch stress-rupture crack led to tensile overload, instability and to the onset of rapid crack propagation in a shear mode, with the initial shear fracture propagating as an extension of the original stress-rupture crack. Within a short distance, this shear fracture turned 90° and propagated in the plate rolling direction, a result explained by the anisotropy of the fracture resistance of this steel at the elevated temperatures of the test.

17. KEY WORDS (six to twelve entries; alphabetical order; capitalize only the first letter of the first key word unless a proper name; separated by semicolons)

Anisotropy; ductile fracture; fire test; insulated rail tank car; stress rupture crack

18. AVAILABILITY	19. SECURITY CLASS (THIS REPORT)	21. NO. OF PAGES
[ ] Unlimited XX For Official Distribution. Do Not Release to NTIS [ ] Order From Sup. of Doc., U.S. Government Printing Office Washington, D.C. 20402, SD Cat. No. C13 [ ] Order From National Technical Information Service (NTIS) Springfield, Virginia 22151	UNCLASSIFIED	63
	20. SECURITY CLASS (THIS PAGE) UNCLASSIFIED	22. Price

USCOMM-DC 29042-P74


AMERICAN REVOLUTION BICENTENNIAL
1776-1976